NONLINEAR ATTITUDE CONTROL OF SPACECRAFT WITH A CAPTURED ASTEROID

Saptarshi Bandyopadhyay*, Soon-Jo Chung†, and Fred Y. Hadaegh‡

One of the main control challenges of National Aeronautics and Space Administration's Asteroid Redirect Mission (ARM) is to stabilize and control the attitude of the spacecraft-asteroid combination in the presence of large uncertainty in the physical model of a captured asteroid. We present a new robust nonlinear tracking control law that guarantees global exponential convergence of the system's attitude trajectory to the desired attitude trajectory. In the presence of modeling errors and disturbances, this control law is finite-gain $\mathcal{L}_p$ stable and input-to-state stable. We also present a few extensions of this control law, such as exponential tracking control on SO(3) and integral control, and show its relation to the well-known tracking control law for Euler-Lagrangian systems. We show that the resultant disturbance torques for control laws that use feed-forward cancellation is comparable to the maximum control torque of the conceptual ARM spacecraft and such control laws are therefore not suitable. We then numerically compare the performance of multiple viable attitude control laws, including the robust nonlinear tracking control law, nonlinear adaptive control, and derivative plus proportional-derivative linear control. We conclude that under very small modeling uncertainties, which can be achieved using online system identification, the robust nonlinear tracking control law that guarantees globally exponential convergence to the fuel-optimal reference trajectory is the best strategy as it consumes the least amount of fuel. On the other hand, in the presence of large modeling uncertainties and actuator saturations, a simple derivative plus proportional-derivative (D+PD) control law is effective, and the performance can be further improved by using the proposed nonlinear tracking control law that tracks a "D+PD"-control-based desired attitude trajectory. We conclude this paper with specific design guidelines for the ARM spacecraft for efficiently stabilizing a tumbling asteroid and spacecraft combination.

INTRODUCTION

Multiple space agencies have announced plans for future small body exploration and hazard mitigation missions.[1,2,3] Recently, European Space Agency's Rosetta spacecraft landed the Philae robotic lander on the nucleus of the comet 67P/Churyumov–Gerasimenko.[4] National Aeronautics and Space Administration's (NASA) Asteroid Redirect Mission (ARM) is targeting carbonaceous Near Earth Orbit (NEO) asteroids, which have diameters between 7-10 m and mass between 2.5-13 $\times$ 10^5 kg, because they could potentially answer questions about the origin of life and provide opportunities for in-situ resource utilization.[5] The objective of the first ARM mission concept is to capture a NEO asteroid or to pick up a boulder from some bigger target asteroid and transport the captured body back to the Earth–Moon system. In this paper, we provide a detailed analysis of one of the main control challenges for the ARM mission concept: despinning and three-axis attitude control of the asteroid and spacecraft combination after the tumbling asteroid is captured by the ARM spacecraft, as shown in Fig. 1(a).[5] In the new ARM mission concept shown in Fig. 1(b),[6,7] the same attitude control problem applies after a boulder is picked up and the spacecraft-boulder combination is separated from a larger asteroid.

*Graduate Research Assistant, Department of Aerospace Engineering, University of Illinois at Urbana-Champaign, Urbana, Illinois, 61801, USA

†Assistant Professor, Department of Aerospace Engineering and Coordinated Science Laboratory, University of Illinois at Urbana-Champaign, Urbana, Illinois, 61801, USA

‡Senior Research Scientist and Technical Fellow, Jet Propulsion Laboratory, California Institute of Technology, Pasadena, California 91109, USA

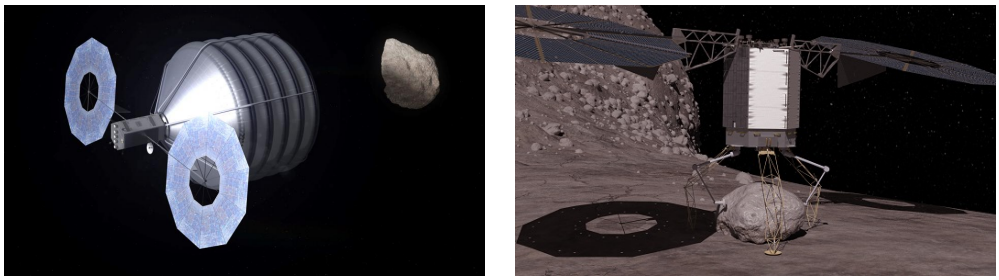

(a) (b)

Figure 1. (a) Artist's rendering of the conceptual ARM spacecraft about to capture a NEO asteroid (image credit: NASA[5]). (b) Artist's rendering of the conceptual ARM spacecraft about to pickup a boulder from a large asteroid (image credit: NASA[7]).

In this paper, we present and compare attitude control strategies for despinning and three-axis stabilizing the asteroid and spacecraft combination after the tumbling asteroid is captured by the ARM spacecraft. In Refs. 8, 9, a simple attitude control strategy is presented for a spacecraft-asteroid combination that assumes perfect knowledge of the asteroid's physical parameters and neglects modeling uncertainties, saturations, and disturbances. In contrast, we present attitude control strategies that stabilize the tumbling asteroid and spacecraft combination in the presence of uncertain physical parameters, bounded disturbances, measurement errors, and actuator saturations. Attitude control with uncertainty is a topic of intense research.[10,11,12,13] For the purpose of achieving large slew-maneuvers and superior tracking performance for a time-varying desired trajectory, nonlinear attitude tracking control should be used in lieu of linear control. In this paper, we show that common nonlinear attitude control laws that use exact feed-forward cancellation, similar to feedback linearization, exhibit a large resultant disturbance torque due to an unprecedentedly large modeling uncertainties of a captured asteroid. In contrast, attitude control laws, which do not have a feed-forward term,[14,15,16] experience a much smaller resultant disturbance torque. We elaborate that the proposed robust nonlinear tracking control law can be designed to exploit the benefit of no feed-forward cancellation while achieving superior tracking performance in the presence of large modeling uncertainties, measurement errors, and actuator saturations.

Paper Contribution

The first main contribution of this paper is the development of a robust nonlinear tracking control law that guarantees global exponential convergence of the system's attitude trajectory to the desired attitude trajectory. In the presence of disturbances, this control law is finite-gain $\mathcal{L}_p$ stable and input-to-state stable. We show that this control law is related to the well-known tracking control law for Euler-Lagrangian systems,[16,14] but the new control law directly prescribes the control torque input with less dependence on the kinematic relationship. This offers several advantages over the EL-based control law. Another advantage of this new control law is that it can be easily extended with an integral control term or an exponentially-stabilizing tracking control law on SO(3) for global attitude representation. We also discuss techniques for generating fuel-optimal and resultant disturbance torque minimizing desired attitude trajectories.

The second main contribution of this paper is to compare the resultant disturbance torques for different types of control laws. We show that control laws that use feed-forward cancellation, experience a resultant disturbance torque that is comparable to the maximum control torque of the conceptual ARM spacecraft and can lead to actuator saturation. Therefore, such control laws are not suitable for an ARM mission type. We also discuss methods for reducing this resultant disturbance torque for the novel robust tracking control law.

The comparison study of the fuel usage and time of convergence of multiple attitude control laws using numerical simulations is also presented. The third main contribution of this paper indicates that the best control strategy under very small modeling uncertainties, which can be achieved using online system identification from both proximity and contact operations, is to track the fuel-optimal reference trajectory using the

globally-exponentially-stabilizing robust nonlinear tracking control law. On the other hand, in the presence of large modeling uncertainties, measurement errors, and actuator saturations, the best control strategy is to use the robust nonlinear tracking control law, which tracks a derivative plus proportional-derivative based desired attitude trajectory. We also provide specific design guidelines for the ARM spacecraft for efficiently stabilizing the asteroid and spacecraft combination.

PRELIMINARIES AND PROBLEM STATEMENT

In this section, we present the attitude kinematics and dynamics of the asteroid and spacecraft combination and then state the control problem statement. Nominal ARM spacecraft design used in this paper is shown in Fig. 2(a). The Reaction Control Subsystem (RCS), which includes includes four pods of four thrusters, will be used for attitude control of the tumbling asteroid and spacecraft combination.

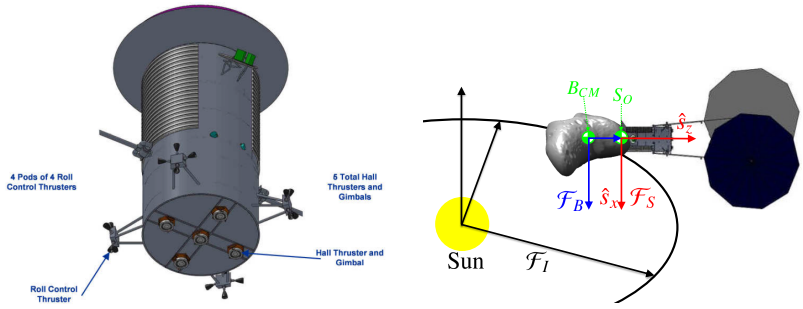

(a) (b)

Figure 2. (a) Bottom view of the conceptual ARM spacecraft with the four RCS thruster pods (image credit: NASA[5]). (b) Reference Frames: the inertial frame $\mathcal{F}_I$, the body fixed frame $\mathcal{F}_B$, and the spacecraft frame $\mathcal{F}_S$.

Attitude Dynamics and Kinematics of the Asteroid and Spacecraft Combination

We assume that the asteroid and ARM spacecraft combination is a tumbling rigid body. Note that the slippage between the capture mechanism and the asteroid and the flexibility of the solar arrays are neglected in this paper. In this section, we present the attitude dynamics and kinematics equations that are used in this paper.

The center of mass of the asteroid and spacecraft combination (B_{CM}) is the origin of the body fixed frame $\mathcal{F}_B$, as shown in Fig. 2(b). Let S_O, which is the base of the ARM-spacecraft's body, be the origin of the spacecraft frame $\mathcal{F}_S$ as shown in Fig. 2(b). We assume that attitude orientation of $\mathcal{F}_B$ with respect to $\mathcal{F}_I$ is the same as that of $\mathcal{F}_S$ with respect to $\mathcal{F}_I$, i.e., the rotation matrix from $\mathcal{F}_S$ to $\mathcal{F}_B$ is an identity matrix. Let $\boldsymbol{r}^{S_O/B_{CM}}$ denote the vector from B_{CM} to S_O.

Let $\boldsymbol{J}_{\text{ast}}^{B_{CM}}$ be the unknown, constant, positive-definite inertia tensor of the asteroid at B_{CM} and expressed in $\mathcal{F}_B$. Let $\boldsymbol{J}_{\text{sc}}^{S_{CM}}$ be the known, constant, positive-definite inertia tensor of the ARM spacecraft at the center of mass of the ARM spacecraft (S_{CM}) and expressed in $\mathcal{F}_S$. The combined inertia tensor of the asteroid and spacecraft combination at B_{CM} and expressed in $\mathcal{F}_B$ is determined using the parallel axis theorem to be:

$$\boldsymbol{J}_{\text{tot}}^{B_{CM}} = \boldsymbol{J}_{\text{ast}}^{B_{CM}} + \boldsymbol{J}_{\text{sc}}^{S_{CM}} + m_{\text{sc}} \left[\left(\boldsymbol{r}^{S_{CM}/B_{CM}} \right)^T \left(\boldsymbol{r}^{S_{CM}/B_{CM}} \right) \mathbf{I} - \left(\boldsymbol{r}^{S_{CM}/B_{CM}} \right) \left(\boldsymbol{r}^{S_{CM}/B_{CM}} \right)^T \right], \tag{1}$$

where $\boldsymbol{r}^{S_{CM}/B_{CM}} = \boldsymbol{r}^{S_{CM}/S_O} + \boldsymbol{r}^{S_O/B_{CM}}$, $\boldsymbol{r}^{S_{CM}/S_O}$ is the known vector from S_O to S_{CM}, m_{sc} is the mass of the spacecraft.

Let $\boldsymbol{\omega} \in \mathbb{R}^3$ be the angular velocity of the asteroid and spacecraft combination in the body fixed frame $\mathcal{F}_B$ with respect to the inertial frame $\mathcal{F}_I$ and expressed in the frame $\mathcal{F}_B$. Let $\boldsymbol{u} \in \mathbb{R}^8$ and $\boldsymbol{B} \in \mathbb{R}^{3\times 8}$ represent

the thrust outputs of the eight thrusters and the control influence matrix. Let $\boldsymbol{d}_{\text{ext}} \in \mathbb{R}^3$ denote the external disturbance torques on the system. The attitude dynamics of the rigid asteroid and spacecraft combination is given by:

$$\boldsymbol{J}_{\text{tot}}^{B_{CM}} \dot{\boldsymbol{\omega}} = \left(\boldsymbol{J}_{\text{tot}}^{B_{CM}} \boldsymbol{\omega} \right) \times \boldsymbol{\omega} + \boldsymbol{B}\boldsymbol{u} + \boldsymbol{d}_{\text{ext}} \,. \tag{2}$$

The attitude kinematics of the rigid asteroid and spacecraft combination using quaternions is given by:[17,18]

$$\dot{\boldsymbol{\beta}}_v = \frac{1}{2}(\beta_4 \boldsymbol{\omega} + \boldsymbol{\beta}_v \times \boldsymbol{\omega}) \,, \qquad \dot{\beta}_4 = -\frac{1}{2}\boldsymbol{\beta}_v^T \boldsymbol{\omega} \,, \tag{3}$$

where $\boldsymbol{\beta}_v = [\beta_1, \beta_2, \beta_3] \in \mathbb{R}^3$ and $\boldsymbol{\beta} = [\boldsymbol{\beta}_v, \beta_4] \in \mathbb{S}^3$. The corresponding attitude kinematics equation using modified Rodrigues parameters (MRP) is given by:[16]

$$\dot{\boldsymbol{q}} = \boldsymbol{Z}(\boldsymbol{q})\boldsymbol{\omega} \,, \quad \text{where} \qquad \boldsymbol{Z}(\boldsymbol{q}) = \frac{1}{2}\left[\mathbf{I}\left(\frac{1 - \boldsymbol{q}^T\boldsymbol{q}}{2} \right) + \boldsymbol{q}\boldsymbol{q}^T + \boldsymbol{S}(\boldsymbol{q}) \right] \,, \quad \boldsymbol{S}(\boldsymbol{q}) = \begin{bmatrix} 0 & -q_3 & q_2 \\ q_3 & 0 & -q_1 \\ -q_2 & q_1 & 0 \end{bmatrix} \tag{4}$$

The attitude kinematics equations using Euler angles, classical Rodrigues parameters, and the quaternion vector ($\boldsymbol{\beta}_v$) can also be written in the form of $\dot{\boldsymbol{q}} = \boldsymbol{Z}(\boldsymbol{q})\boldsymbol{\omega}$ (like Eq. (4)) with a different definition of $\boldsymbol{Z}(\boldsymbol{q})$.[19] The attitude kinematics of a rotation matrix on SO(3) is given by:

$$\dot{\boldsymbol{R}} = \boldsymbol{R}\boldsymbol{S}(\boldsymbol{\omega}) \,, \tag{5}$$

where $\boldsymbol{R}$ represents the rotation of the body fixed frame $\mathcal{F}_B$ with respect to the inertial frame $\mathcal{F}_I$.

We now study the effect of modeling uncertainties in $\boldsymbol{J}_{\text{ast}}^{B_{CM}}$ and $\boldsymbol{r}^{S_O/B_{CM}}$, measurement errors in $\boldsymbol{\omega}$, and actuator errors in $\boldsymbol{u}$ on the attitude dynamics of the asteroid and spacecraft combination (2). Let $\boldsymbol{J}_{\text{ast}}^{B_{CM}} = \hat{\boldsymbol{J}}_{\text{ast}}^{B_{CM}} + \Delta\boldsymbol{J}_{\text{ast}}^{B_{CM}}$, where $\hat{\boldsymbol{J}}_{\text{ast}}^{B_{CM}}$ is the estimated inertia tensor of the asteroid and $\Delta\boldsymbol{J}_{\text{ast}}^{B_{CM}}$ is the modeling error. Similarly, let $\boldsymbol{r}^{S_O/B_{CM}} = \hat{\boldsymbol{r}}^{S_O/B_{CM}} + \Delta\boldsymbol{r}^{S_O/B_{CM}}$. The true angular velocity $\boldsymbol{\omega}$ is decomposed as $\boldsymbol{\omega} = \hat{\boldsymbol{\omega}} + \Delta\boldsymbol{\omega}$, where $\hat{\boldsymbol{\omega}}$ is the measured angular velocity and $\Delta\boldsymbol{\omega}$ is the measurement error. Finally, the true thruster output is written as $\boldsymbol{u} = \hat{\boldsymbol{u}} + \Delta\boldsymbol{u}$, where $\hat{\boldsymbol{u}}$ is the thruster output commanded by the control law and $\Delta\boldsymbol{u}$ is the actuator error. Due to these uncertainties and errors, we get $\boldsymbol{J}_{\text{tot}}^{B_{CM}} = \hat{\boldsymbol{J}}_{\text{tot}}^{B_{CM}} + \Delta\boldsymbol{J}_{\text{tot}}^{B_{CM}}$ and $\boldsymbol{B} = \hat{\boldsymbol{B}} + \Delta\boldsymbol{B}$. Simplifying the dynamics of the asteroid and spacecraft combination (2) gives:

$$(\hat{\boldsymbol{J}}_{\text{tot}}^{B_{CM}} + \Delta\boldsymbol{J}_{\text{tot}}^{B_{CM}})\dot{\hat{\boldsymbol{\omega}}} - (\hat{\boldsymbol{J}}_{\text{tot}}^{B_{CM}} + \Delta\boldsymbol{J}_{\text{tot}}^{B_{CM}})\hat{\boldsymbol{\omega}} \times \hat{\boldsymbol{\omega}} = \boldsymbol{u}_c + \boldsymbol{d}_{\text{res}} \tag{6}$$

where $\boldsymbol{u}_c = \hat{\boldsymbol{B}}\hat{\boldsymbol{u}}$ and $\boldsymbol{d}_{\text{res}} = \left(\hat{\boldsymbol{J}}_{\text{tot}}^{B_{CM}} + \Delta\boldsymbol{J}_{\text{tot}}^{B_{CM}} \right) \Delta\boldsymbol{\omega} \times \hat{\boldsymbol{\omega}} + \left(\hat{\boldsymbol{J}}_{\text{tot}}^{B_{CM}} + \Delta\boldsymbol{J}_{\text{tot}}^{B_{CM}} \right) \hat{\boldsymbol{\omega}} \times \Delta\boldsymbol{\omega} + \Delta\boldsymbol{B}\hat{\boldsymbol{u}} + \hat{\boldsymbol{B}}\Delta\boldsymbol{u} - \hat{\boldsymbol{J}}_{\text{tot}}^{B_{CM}}\Delta\dot{\boldsymbol{\omega}} + \boldsymbol{d}_{\text{ext}}$. Note that $\Delta\boldsymbol{J}_{\text{tot}}^{B_{CM}}$ is the only unknown parameter in the left hand side of Eq. (6). We use Eq. (6) to analyze the stability of control laws presented in this paper. A detailed study of the resultant disturbance torques for different control laws is presented later on.

Problem Statement: Attitude Control of the Asteroid and Spacecraft Combination

The salient features of the attitude control problem discussed in this paper are as follows: (i) The asteroid and ARM spacecraft combination is tumbling. The tumbling rate can be nonuniform due to the cross-terms in the moment of inertia tensor. (ii) The asteroid's inertia tensor, mass, center of mass, and center of gravity have large uncertainties (approximately 10% of the nominal value). (iii) The asteroid is non-collaborative; i.e., no actuators are placed on the asteroid. All actuators are on board the ARM spacecraft.

Let $\boldsymbol{q}_{\text{final}}$ denote the desired attitude orientation of the stabilized system. The attitude control objective is to detumble and control the attitude dynamics of the asteroid and spacecraft combination. The control objective is to stabilize the system, in the presence of uncertain physical parameters, bounded disturbances, measurement errors, and actuator saturations, such that for some appropriate $\varepsilon_{\text{trans}} > 0$, $\varepsilon_{\text{ss}} > 0$, and $T \gg 0$:

$$\|\boldsymbol{\omega}(t)\|_2 \leq \varepsilon_{\text{trans}}, \qquad \forall t > 0 \,, \tag{7}$$

$$\|\boldsymbol{q}(t) - \boldsymbol{q}_{\text{final}}\|_2 \leq \varepsilon_{\text{ss}}, \qquad \forall t > T \,. \tag{8}$$

The transient error bound $\varepsilon_{\text{trans}}$ is imposed on the angular velocity $\boldsymbol{\omega}(t)$ in Eq. (7) in order to ensure that the system is always within the technological capability of the sensors and actuators on board the ARM spacecraft. It is desired that after time T, the asteroid and spacecraft combination should achieve the desired attitude orientation $\boldsymbol{q}_{\text{final}}$ as shown in the steady-state condition (8). Note that if the system has to hold its attitude within the given steady-state error bound ε_{ss}, then the desired angular velocity $\boldsymbol{\omega}_{\text{final}}$ of the stabilized system should be sufficiently close to $\mathbf{0}$ rad sec^{-1}.

In this paper, a control law that guarantees global exponential convergence or a contracting closed-loop dynamics is derived to achieve the objectives in Eqs. (7-8). Hence, in the presence of disturbances, such a globally exponentially stabilizing control law yields finite-gain $\mathcal{L}_p$ stability and input-to-state stability.[20] If a control law that only yields global asymptotic convergence (without any disturbance), then the error in the system's trajectory may not be bounded for a certain class of disturbance or proving robustness is more involved.[20]

CONTROL LAWS FOR NONLINEAR ATTITUDE CONTROL

In this section, we present various control laws that are deemed suitable for satisfying the control problem statement. We first present a novel robust nonlinear tracking control law that guarantees globally exponential convergence of the system's attitude to the desired attitude. In order to highlight the advantages of this new control law, we also present several extensions of this attitude tracking control law, like augmenting it with an integral control term and deriving an exponentially-stabilizing tracking control law on SO(3). We also discuss techniques for computing the fuel-optimal desired attitude trajectory and and the resultant disturbance torque minimizing desired attitude trajectory, which is based on the derivative plus proportional-derivative control strategy.

Robust Nonlinear Tracking Control Law with Global Exponential Stability

The following theorem states the proposed robust nonlinear tracking control law, which directly computes the control input $\boldsymbol{u}_c$ for (6). Note that this control law does not cancel the term $\boldsymbol{S}\left(\hat{\boldsymbol{J}}_{\text{tot}}^{B_{CM}}\hat{\boldsymbol{\omega}}\right)\hat{\boldsymbol{\omega}}$ exactly, in contrast with most conventional nonlinear tracking control laws using feed-forward cancellation.[12,21] The effect of this feed-forward cancellation on the resultant disturbance torque is discussed in detail in Section . Although this control law is written for MRP, it can also be used with other attitude representations like Euler angles, classical Rodrigues parameters, and the quaternion vector, by changing the definition of $\boldsymbol{Z}(\boldsymbol{q})$.

Theorem 1. For the given desired attitude trajectory $\boldsymbol{q}_d(t)$, and positive definite constant matrices $\boldsymbol{K}_r \in \mathbb{R}^{3\times3}$ and $\boldsymbol{\Lambda}_r \in \mathbb{R}^{3\times3}$, we define the following control law:

$$\begin{aligned} \boldsymbol{u}_c &= \hat{\boldsymbol{J}}_{\text{tot}}^{B_{CM}}\dot{\boldsymbol{\omega}}_r - \boldsymbol{S}\left(\hat{\boldsymbol{J}}_{\text{tot}}^{B_{CM}}\hat{\boldsymbol{\omega}}\right)\boldsymbol{\omega}_r - \boldsymbol{K}_r(\hat{\boldsymbol{\omega}} - \boldsymbol{\omega}_r)\,, \\ \text{where}\quad \boldsymbol{\omega}_r &= \boldsymbol{Z}^{-1}(\hat{\boldsymbol{q}})\dot{\boldsymbol{q}}_d(t) + \boldsymbol{Z}^{-1}(\hat{\boldsymbol{q}})\boldsymbol{\Lambda}_r(\boldsymbol{q}_d(t) - \hat{\boldsymbol{q}})\,. \end{aligned} \tag{9}$$

This control law stabilizes the asteroid and spacecraft combination (6) and has the following properties:
(i) In the absence of resultant disturbance torque, this control law guarantees global exponential convergence of the system's trajectory to the desired trajectory $\boldsymbol{q}_d(t)$.
(ii) In the presence of bounded resultant disturbance torque, this control law guarantees the system's trajectory will globally exponentially converge to a bounded error ball around the desired trajectory $\boldsymbol{q}_d(t)$. Hence, this control law is finite-gain $\mathcal{L}_p$ stable and input-to-state stable (ISS), which are sufficient conditions for satisfying the control problem statement Eqs. (7-8).

Proof: The closed-loop dynamics, which is obtained by substituting $\boldsymbol{u}_c$ from Eq. (9) into Eq. (6), becomes

$$\boldsymbol{J}_{\text{tot}}^{B_{CM}}\dot{\boldsymbol{\omega}}_e - \boldsymbol{S}\left(\boldsymbol{J}_{\text{tot}}^{B_{CM}}\hat{\boldsymbol{\omega}}\right)\boldsymbol{\omega}_e + \boldsymbol{K}_r\boldsymbol{\omega}_e = \underbrace{\left[\boldsymbol{d}_{\text{res}} + \Delta\boldsymbol{J}_{\text{tot}}^{B_{CM}}\dot{\boldsymbol{\omega}}_r - \boldsymbol{S}\left(\Delta\boldsymbol{J}_{\text{tot}}^{B_{CM}}\hat{\boldsymbol{\omega}}\right)\boldsymbol{\omega}_r\right]}_{\boldsymbol{d}_{\text{res},1}}, \tag{10}$$

where $\boldsymbol{\omega}_e = (\hat{\boldsymbol{\omega}} - \boldsymbol{\omega}_r)$. The new resultant disturbance, $\boldsymbol{d}_{\text{res},1}$ is different from $\boldsymbol{d}_{\text{res}}$ used in Eq. (6). Let us first show that the control law indeed globally exponentially stabilizes the closed-loop system, without the resultant disturbance $\boldsymbol{d}_{\text{res},1}$. The virtual dynamics of $\boldsymbol{y}$, derived from Eq. (10) without $\boldsymbol{d}_{\text{res},1}$, is given as

$$\boldsymbol{J}_{\text{tot}}^{B_{CM}} \dot{\boldsymbol{y}} - \boldsymbol{S}\left(\boldsymbol{J}_{\text{tot}}^{B_{CM}} \hat{\boldsymbol{\omega}}\right) \boldsymbol{y} + \boldsymbol{K}_r \boldsymbol{y} = \boldsymbol{0}\,, \tag{11}$$

where $\boldsymbol{y}$ has $\boldsymbol{y} = \boldsymbol{\omega}_e$ and $\boldsymbol{y} = \boldsymbol{0}$ as its two particular solutions. After we obtain the dynamics of the infinitesimal displacement at fixed time, $\delta\boldsymbol{y}$ from (11), we perform the squared-length analysis:

$$\frac{d}{dt}\left(\delta \boldsymbol{y}^T \boldsymbol{J}_{\text{tot}}^{B_{CM}} \delta \boldsymbol{y}\right) = -2\delta \boldsymbol{y}^T \boldsymbol{K}_r \delta \boldsymbol{y} \leq \frac{-2\lambda_{\min}(\boldsymbol{K}_r)}{\lambda_{\max}(\boldsymbol{J}_{\text{tot}}^{B_{CM}})}\left(\delta \boldsymbol{y}^T \boldsymbol{J}_{\text{tot}}^{B_{CM}} \delta \boldsymbol{y}\right)\,. \tag{12}$$

Hence, it follows from the contraction analysis (Lemma 3 in Ref. 22) that all system trajectories of (11) converge exponentially fast to a single trajectory (i.e., $\delta\boldsymbol{y} \to \boldsymbol{0}$ and $\boldsymbol{\omega}_e \to \boldsymbol{0}$) at a rate of $\frac{\lambda_{\min}(\boldsymbol{K}_r)}{\lambda_{\max}(\boldsymbol{J}_{\text{tot}}^{B_{CM}})}$.

In the presence of bounded resultant disturbance $\boldsymbol{d}_{\text{res},1}$, it follows from Lemma 4 in Ref. 13 that:

$$\lim_{t\to\infty} \int_0^{\boldsymbol{\omega}_e} \|\delta \boldsymbol{y}\|_2 \leq \frac{\lambda_{\max}(\boldsymbol{J}_{\text{tot}}^{B_{CM}})}{\lambda_{\min}(\boldsymbol{K}_r)\lambda_{\min}(\boldsymbol{J}_{\text{tot}}^{B_{CM}})} \sup_t \|\boldsymbol{d}_{\text{res},1}\|_2 \tag{13}$$

Hence the dynamics of the closed-loop system is bounded in the presence of bounded resultant disturbance $\boldsymbol{d}_{\text{res},1}$. We now prove that convergence of $\boldsymbol{\omega}_e \to \boldsymbol{0}$ implies convergence of the system's trajectory to the desired trajectory ($\hat{\boldsymbol{q}} \to \boldsymbol{q}_d$). It follows from the definition of $\boldsymbol{\omega}_r$ that:

$$\boldsymbol{\omega}_e = \boldsymbol{Z}^{-1}(\hat{\boldsymbol{q}})(\dot{\hat{\boldsymbol{q}}} - \dot{\boldsymbol{q}}_d) + \boldsymbol{Z}^{-1}(\hat{\boldsymbol{q}})\boldsymbol{\Lambda}_r(\hat{\boldsymbol{q}} - \boldsymbol{q}_d) = \boldsymbol{Z}^{-1}(\hat{\boldsymbol{q}})(\dot{\boldsymbol{q}}_e + \boldsymbol{\Lambda}_r \boldsymbol{q}_e)\,, \tag{14}$$

where $\boldsymbol{q}_e = (\hat{\boldsymbol{q}} - \boldsymbol{q}_d)$. In the absence of $\boldsymbol{\omega}_e$, all system trajectories of $\delta\boldsymbol{q}_e$ will converge exponentially fast to a single trajectory ($\delta\boldsymbol{q}_e \to 0$) with a rate of $\lambda_{\min}(\boldsymbol{\Lambda}_r)$, where the virtual displacement $\delta\boldsymbol{q}_e$ is an infinitesimal displacement at fixed time. In the presence of $\boldsymbol{\omega}_e$, it follows from Lemma 4[13] that:

$$\begin{aligned}\lim_{t\to\infty} \int_0^{\boldsymbol{q}_e} \|\delta \boldsymbol{q}_e\|_2 &\leq \frac{1}{\lambda_{\min}(\boldsymbol{\Lambda}_r)} \sup_t \|\boldsymbol{Z}(\hat{\boldsymbol{q}})\boldsymbol{\omega}_e\|_2 \\ &\leq \frac{\lambda_{\max}(\boldsymbol{J}_{\text{tot}}^{B_{CM}})}{\lambda_{\min}(\boldsymbol{\Lambda}_r)\lambda_{\min}(\boldsymbol{K}_r)\lambda_{\min}(\boldsymbol{J}_{\text{tot}}^{B_{CM}})}\left(\sup_t \sigma_{\max}(\boldsymbol{Z}(\hat{\boldsymbol{q}}))\right)\left(\sup_t \|\boldsymbol{d}_{\text{res},1}\|_2\right)\,.\end{aligned} \tag{15}$$

Hence we have shown, by constructing a hierarchically-combined closed-loop system of $\boldsymbol{\omega}_e$ and $\boldsymbol{q}_e$, that the attitude trajectory $\boldsymbol{q}$ will globally exponentially converge to a bounded error ball around the desired trajectory $\boldsymbol{q}_d(t)$. Moreover, it follows from Lemma 4[13] that this control law is finite-gain $\mathcal{L}_p$ stable and input-to-state stable (ISS). Hence the control gains $\boldsymbol{K}_r$ and $\boldsymbol{\Lambda}_r$ can be designed such that the error bounds $\varepsilon_{\text{trans}}$ and ε_{ss} in Eqs. (7-8) are satisfied. ■

The desired attitude trajectory $\boldsymbol{q}_d(t)$ can be any reference trajectory that we would like the system to track. WThe actual thruster inputs $\hat{\boldsymbol{u}}$ are generated from this control torque input $\boldsymbol{u}_c$ using the Moore–Penrose pseudoinverse of $\hat{\boldsymbol{B}}$.

Relation to Nonlinear Tracking Control using Euler-Lagrangian Systems

In this section, we compare the robust nonlinear tracking control law Eq. (9) with the well-known robust nonlinear tracking control for Euler-Lagrangian (EL) systems.[14] Let us first state the EL system with uncertainty, which is a combined representation of the attitude kinematics and dynamics of the system:

$$\hat{\boldsymbol{M}}(\hat{\boldsymbol{q}})\ddot{\hat{\boldsymbol{q}}} + \hat{\boldsymbol{C}}(\hat{\boldsymbol{q}}, \dot{\hat{\boldsymbol{q}}})\dot{\hat{\boldsymbol{q}}} = \hat{\boldsymbol{\tau}}_c + \boldsymbol{\tau}_{\text{res}}\,, \tag{16}$$

$$\text{where} \quad \hat{\boldsymbol{\tau}}_c = \boldsymbol{Z}^{-T}(\hat{\boldsymbol{q}})\boldsymbol{u}_c\,, \qquad \hat{\boldsymbol{M}}(\hat{\boldsymbol{q}}) = \boldsymbol{Z}^{-T}(\hat{\boldsymbol{q}})\hat{\boldsymbol{J}}_{\text{tot}}^{B_{CM}}\boldsymbol{Z}^{-1}(\hat{\boldsymbol{q}})\,,$$

$$\hat{\boldsymbol{C}}(\hat{\boldsymbol{q}}, \dot{\hat{\boldsymbol{q}}}) = -\boldsymbol{Z}^{-T}(\hat{\boldsymbol{q}})\hat{\boldsymbol{J}}_{\text{tot}}^{B_{CM}}\boldsymbol{Z}^{-1}(\hat{\boldsymbol{q}})\dot{\boldsymbol{Z}}(\hat{\boldsymbol{q}})\boldsymbol{Z}^{-1}(\hat{\boldsymbol{q}}) - \boldsymbol{Z}^{-T}(\hat{\boldsymbol{q}})\,\boldsymbol{S}\left(\hat{\boldsymbol{J}}_{\text{tot}}^{B_{CM}}\boldsymbol{Z}^{-1}(\hat{\boldsymbol{q}})\dot{\hat{\boldsymbol{q}}}\right)\boldsymbol{Z}^{-1}(\hat{\boldsymbol{q}})\,,$$

and $\boldsymbol{\tau}_{\text{res}}$ is the resultant disturbance torque acting on the EL system. Note that $\dot{\hat{\boldsymbol{M}}}(\hat{\boldsymbol{q}}) - 2\hat{\boldsymbol{C}}(\hat{\boldsymbol{q}}, \dot{\hat{\boldsymbol{q}}})$ in Eq. (16) is a skew-symmetric matrix, and this property is essential to the stability proof. Let us use a slight modification of the original robust nonlinear tracking control law Eq. (9), which is given by:

$$\boldsymbol{u}_c = \hat{\boldsymbol{J}}_{\text{tot}}^{B_{CM}} \dot{\boldsymbol{\omega}}_r - \boldsymbol{S}\left(\hat{\boldsymbol{J}}_{\text{tot}}^{B_{CM}} \hat{\boldsymbol{\omega}}\right) \boldsymbol{\omega}_r - \boldsymbol{Z}^T(\hat{\boldsymbol{q}}) \boldsymbol{K}_\ell \boldsymbol{Z}(\hat{\boldsymbol{q}})(\hat{\boldsymbol{\omega}} - \boldsymbol{\omega}_r) \tag{17}$$

where $\boldsymbol{K}_\ell \in \mathbb{R}^{3\times3}$ and $\boldsymbol{\Lambda}_\ell \in \mathbb{R}^{3\times3}$ are positive definite constant matrices. Substituting $\boldsymbol{\omega}_r$ into (17), using the identity $\dot{\boldsymbol{Z}}^{-1}(\hat{\boldsymbol{q}}) = -\boldsymbol{Z}^{-1}(\hat{\boldsymbol{q}}) \dot{\boldsymbol{Z}}(\hat{\boldsymbol{q}}) \boldsymbol{Z}^{-1}(\hat{\boldsymbol{q}})$, and multiplying both sides with $\boldsymbol{Z}^{-T}(\hat{\boldsymbol{q}})$ gives us:

$$\hat{\boldsymbol{\tau}}_c = \hat{\boldsymbol{M}}(\hat{\boldsymbol{q}}) \ddot{\boldsymbol{q}}_r + \hat{\boldsymbol{C}}(\hat{\boldsymbol{q}}, \dot{\hat{\boldsymbol{q}}}) \dot{\boldsymbol{q}}_r - \boldsymbol{K}_\ell (\dot{\hat{\boldsymbol{q}}} - \dot{\boldsymbol{q}}_r)\,, \tag{18}$$

where $\dot{\boldsymbol{q}}_r = \dot{\boldsymbol{q}}_d(t) + \boldsymbol{\Lambda}_\ell(\boldsymbol{q}_d(t) - \hat{\boldsymbol{q}})$.

Remark 1. (*Advantages of original control law (9) over this control law for EL system (18)*): The control law for EL system (18) extensively uses the measured attitude $\hat{\boldsymbol{q}}$ and its rate $\dot{\hat{\boldsymbol{q}}}$ but does not explicitly use the measured angular velocity $\hat{\boldsymbol{\omega}}$. Moreover, the matrices $\boldsymbol{Z}(\hat{\boldsymbol{q}})$ and $\boldsymbol{Z}^{-1}(\hat{\boldsymbol{q}})$, which might be susceptible to large fluctuations due to measurement errors in $\hat{\boldsymbol{q}}$, are used multiple times in Eq. (18). For example, the actual control input $\boldsymbol{u}_c$ depends on the computed control signal $\hat{\boldsymbol{\tau}}_c$ in Eq. (18) through the relation $\boldsymbol{u}_c = \boldsymbol{Z}^T(\hat{\boldsymbol{q}})\hat{\boldsymbol{\tau}}_c$ as shown in Eq. (16). On the other hand, the original control law (9) directly computes $\boldsymbol{u}_c$.

In Eqs. (17) and (18), the terms $\boldsymbol{Z}^T(\hat{\boldsymbol{q}})\boldsymbol{K}_\ell\boldsymbol{Z}$, $\hat{\boldsymbol{M}}(\hat{\boldsymbol{q}})$, and $\hat{\boldsymbol{C}}(\hat{\boldsymbol{q}}, \dot{\hat{\boldsymbol{q}}})$ strongly couple the three axes motions using the highly non-diagonal, non-symmetric matrix $\boldsymbol{Z}(\hat{\boldsymbol{q}})$. This strong coupling of the three-axis rotational motions might be undesirable. For example, initially there might be an error in only one axis, but this coupling will subsequently introduce errors in all three axes. Depending on the inertial matrix, this strong coupling of three-axis motions can be avoided in the proposed control law Eq. (9). □

Robust Nonlinear Tracking Control Law with Integral Control

Another benefit of the original robust nonlinear tracking control law Eq. (9) is that it can be augmented with an integral control term in a straight-forward manner to eliminate any constant external disturbance while ensuring exponential convergence of the system's attitude trajectory to the desired attitude trajectory $\boldsymbol{q}_d(t)$ designed in Sections or .

Theorem 2. For the given desired attitude trajectory $\boldsymbol{q}_d(t)$, positive definite constant matrices $\boldsymbol{K}_m \in \mathbb{R}^{3\times3}$ and $\boldsymbol{\Lambda}_m \in \mathbb{R}^{3\times3}$, and (possibly time-varying) uniformly positive definite diagonal matrix $\boldsymbol{K}_I(t) \in \mathbb{R}^{3\times3}$, we define the following control law:

$$\boldsymbol{u}_c = \hat{\boldsymbol{J}}_{\text{tot}}^{B_{CM}} \dot{\boldsymbol{\omega}}_r - \boldsymbol{S}\left(\hat{\boldsymbol{J}}_{\text{tot}}^{B_{CM}} \hat{\boldsymbol{\omega}}\right) \boldsymbol{\omega}_r - \boldsymbol{K}_m(\hat{\boldsymbol{\omega}} - \boldsymbol{\omega}_r) - \int_0^t \boldsymbol{K}_I(\hat{\boldsymbol{\omega}} - \boldsymbol{\omega}_r) dt\,, \tag{19}$$

$$\text{where} \quad \boldsymbol{\omega}_r = \boldsymbol{Z}^{-1}(\hat{\boldsymbol{q}})\dot{\boldsymbol{q}}_d(t) + \boldsymbol{Z}^{-1}(\hat{\boldsymbol{q}})\boldsymbol{\Lambda}_m(\boldsymbol{q}_d(t) - \hat{\boldsymbol{q}})\,.$$

This control law has the following properties:
(i) This control law always eliminates any constant external disturbance (constant bias) acting on the system.
(ii) If either both $\boldsymbol{K}_I$ and $\dot{\boldsymbol{K}}_I$ are uniformly positive definite diagonal matrices or $\boldsymbol{K}_I$ is a constant positive definite diagonal matrix, then this control law guarantees global exponential convergence of the system's trajectory to the desired trajectory $\boldsymbol{q}_d(t)$ in the absence of time-varying disturbances or uncertainties. Moreover, in the presence of such time-varying bounded disturbances or uncertainties, this control law guarantees that $\boldsymbol{q}$ globally exponentially converge to a bounded error ball around the desired trajectory $\boldsymbol{q}_d(t)$. Hence, by Lemma 4,[13] this control law is also finite-gain $\mathcal{L}_p$ stable and input-to-state stable (ISS).

Proof: The closed-loop dynamics, which is obtained by substituting $\boldsymbol{u}_c$ from Eq. (19) into Eq. (6), is given by:

$$\boldsymbol{J}_{\text{tot}}^{B_{CM}} \dot{\boldsymbol{\omega}}_e - \boldsymbol{S}\left(\boldsymbol{J}_{\text{tot}}^{B_{CM}} \hat{\boldsymbol{\omega}}\right) \boldsymbol{\omega}_e + \boldsymbol{K}_m \boldsymbol{\omega}_e + \int_0^t \boldsymbol{K}_I \boldsymbol{\omega}_e dt = \boldsymbol{d}_{\text{res},1}\,, \tag{20}$$

where $\boldsymbol{\omega}_e = (\hat{\boldsymbol{\omega}} - \boldsymbol{\omega}_r)$ and $\boldsymbol{d}_{\text{res},1}$ is defined in Eq. (10). Let us first show that this control law can eliminate a constant external disturbance, hence removing $\boldsymbol{d}_{\text{res},1}$ from Eq. (20) and adding a constant disturbance term $\boldsymbol{d}_{\text{const}}$ gives us:

$$\boldsymbol{J}_{\text{tot}}^{B_{CM}}\dot{\boldsymbol{\omega}}_e - \boldsymbol{S}\left(\boldsymbol{J}_{\text{tot}}^{B_{CM}}\hat{\boldsymbol{\omega}}\right)\boldsymbol{\omega}_e + \boldsymbol{K}_m\boldsymbol{\omega}_e + \int_0^t \boldsymbol{K}_I\boldsymbol{\omega}_e dt = \boldsymbol{d}_{\text{const}}\,. \tag{21}$$

Differentiating Eq. (21) with respect to time and setting $\dot{\boldsymbol{d}}_{\text{const}} = 0$, we get:

$$\boldsymbol{J}_{\text{tot}}^{B_{CM}}\ddot{\boldsymbol{\omega}}_e + \left(\boldsymbol{K}_m - \boldsymbol{S}\left(\boldsymbol{J}_{\text{tot}}^{B_{CM}}\hat{\boldsymbol{\omega}}\right)\right)\dot{\boldsymbol{\omega}}_e + \left(\boldsymbol{K}_I - \boldsymbol{S}\left(\boldsymbol{J}_{\text{tot}}^{B_{CM}}\dot{\hat{\boldsymbol{\omega}}}\right)\right)\boldsymbol{\omega}_e = 0\,. \tag{22}$$

If we show that Eq. (22) is contracting, then we prove our claim (i) that the given control law can successfully eliminate any constant external disturbance acting on the system. In order to prove Eq. (22) is stable, we consider two cases which depend on the time-varying nature of the matrix $\boldsymbol{K}_I$.

Let us first consider the case where $\boldsymbol{K}_I$ is a constant positive definite diagonal matrix. The matrix $\boldsymbol{K}_I$ can be decomposed into $\boldsymbol{K}_I = \boldsymbol{K}_I^{\frac{1}{2}}\boldsymbol{K}_I^{\frac{1}{2}}$, where the matrix $\boldsymbol{K}_I^{\frac{1}{2}}$ is also a constant positive definite diagonal matrix. Let us introduce the term $\boldsymbol{y}_1$, where $\dot{\boldsymbol{y}}_1$ is defined as $\dot{\boldsymbol{y}}_1 = \boldsymbol{K}_I^{\frac{1}{2}}\boldsymbol{\omega}_e$. Then we can write $\dot{\boldsymbol{\omega}}_e$ as:

$$\dot{\boldsymbol{\omega}}_e = -(\boldsymbol{J}_{\text{tot}}^{B_{CM}})^{-1}\left(\boldsymbol{K}_m - \boldsymbol{S}\left(\boldsymbol{J}_{\text{tot}}^{B_{CM}}\hat{\boldsymbol{\omega}}\right)\right)\boldsymbol{\omega}_e - (\boldsymbol{J}_{\text{tot}}^{B_{CM}})^{-1}\boldsymbol{K}_I^{\frac{1}{2}}\boldsymbol{y}_1\,. \tag{23}$$

Note that differentiating Eq. (23) with respect to time and substituting $\dot{\boldsymbol{y}}_1$ gives us Eq. (22). Therefore, these equations can be written in matrix form as:

$$\begin{bmatrix} \dot{\boldsymbol{\omega}}_e \\ \dot{\boldsymbol{y}}_1 \end{bmatrix} = \underbrace{\begin{bmatrix} -(\boldsymbol{J}_{\text{tot}}^{B_{CM}})^{-1}\left(\boldsymbol{K}_m - \boldsymbol{S}\left(\boldsymbol{J}_{\text{tot}}^{B_{CM}}\hat{\boldsymbol{\omega}}\right)\right) & -(\boldsymbol{J}_{\text{tot}}^{B_{CM}})^{-1}\boldsymbol{K}_I^{\frac{1}{2}} \\ \boldsymbol{K}_I^{\frac{1}{2}} & \boldsymbol{0} \end{bmatrix}}_{\boldsymbol{F}} \begin{bmatrix} \boldsymbol{\omega}_e \\ \boldsymbol{y}_1 \end{bmatrix}. \tag{24}$$

Let us define the positive definite matrix $\boldsymbol{\Xi} = \begin{bmatrix} \boldsymbol{J}_{\text{tot}}^{B_{CM}} & b\mathbf{I} \\ b\mathbf{I} & \mathbf{I} \end{bmatrix}$, where b is a constant between $0 < b < \lambda_{\max}^{\frac{1}{2}}(\boldsymbol{J}_{\text{tot}}^{B_{CM}})$. The symmetric matrix $(\boldsymbol{\Xi F})_{\text{sym}} = \frac{1}{2}\left((\boldsymbol{\Xi F}) + (\boldsymbol{\Xi F})^T\right)$ is given by:

$$(\boldsymbol{\Xi F})_{\text{sym}} = -\begin{bmatrix} \frac{\boldsymbol{K}_m + \boldsymbol{K}_m^T}{2} - b\boldsymbol{K}_I^{\frac{1}{2}} & \frac{b}{2}\left[(\boldsymbol{J}_{\text{tot}}^{B_{CM}})^{-1}\left(\boldsymbol{K}_m - \boldsymbol{S}\left(\boldsymbol{J}_{\text{tot}}^{B_{CM}}\hat{\boldsymbol{\omega}}\right)\right)\right]^T \\ \frac{b}{2}(\boldsymbol{J}_{\text{tot}}^{B_{CM}})^{-1}\left(\boldsymbol{K}_m - \boldsymbol{S}\left(\boldsymbol{J}_{\text{tot}}^{B_{CM}}\hat{\boldsymbol{\omega}}\right)\right) & \frac{b}{2}\left((\boldsymbol{J}_{\text{tot}}^{B_{CM}})^{-1}\boldsymbol{K}_I^{\frac{1}{2}} + \boldsymbol{K}_I^{\frac{1}{2}}(\boldsymbol{J}_{\text{tot}}^{B_{CM}})^{-1}\right) \end{bmatrix}.$$

The sufficient conditions for the matrix $(\boldsymbol{\Xi F})_{\text{sym}}$ to be negative definite are:[23]

$$-\frac{\boldsymbol{K}_m + \boldsymbol{K}_m^T}{2} + b\boldsymbol{K}_I^{\frac{1}{2}} < 0\,, \qquad -\frac{b}{2}\left((\boldsymbol{J}_{\text{tot}}^{B_{CM}})^{-1}\boldsymbol{K}_I^{\frac{1}{2}} + \boldsymbol{K}_I^{\frac{1}{2}}(\boldsymbol{J}_{\text{tot}}^{B_{CM}})^{-1}\right) < 0\,, \tag{25}$$

$$\lambda_{\max}\left(-\frac{\boldsymbol{K}_m + \boldsymbol{K}_m^T}{2} + b\boldsymbol{K}_I^{\frac{1}{2}}\right)\lambda_{\max}\left(-\frac{b}{2}\left((\boldsymbol{J}_{\text{tot}}^{B_{CM}})^{-1}\boldsymbol{K}_I^{\frac{1}{2}} + \boldsymbol{K}_I^{\frac{1}{2}}(\boldsymbol{J}_{\text{tot}}^{B_{CM}})^{-1}\right)\right) > \sigma_{\max}^2\left(-\frac{b}{2}\left[(\boldsymbol{J}_{\text{tot}}^{B_{CM}})^{-1}\left(\boldsymbol{K}_m - \boldsymbol{S}\left(\boldsymbol{J}_{\text{tot}}^{B_{CM}}\hat{\boldsymbol{\omega}}\right)\right)\right]^T\right). \tag{26}$$

Eq. (25) is satisfied by $0 < b < \frac{\lambda_{\min}(\boldsymbol{K}_m + \boldsymbol{K}_m^T)}{2\lambda_{\max}(\boldsymbol{K}_I^{\frac{1}{2}})}$. Eq. (26) is satisfied by $b < b_3$, where b_3 is given by:

$$b_3 = \frac{\lambda_{\max}\left(\frac{\boldsymbol{K}_m + \boldsymbol{K}_m^T}{2}\right)\lambda_{\min}\left((\boldsymbol{J}_{\text{tot}}^{B_{CM}})^{-1}\boldsymbol{K}_I^{\frac{1}{2}} + \boldsymbol{K}_I^{\frac{1}{2}}(\boldsymbol{J}_{\text{tot}}^{B_{CM}})^{-1}\right)}{\frac{1}{2}\sigma_{\max}^2\left[(\boldsymbol{J}_{\text{tot}}^{B_{CM}})^{-1}\left(\boldsymbol{K}_m - \boldsymbol{S}\left(\boldsymbol{J}_{\text{tot}}^{B_{CM}}\hat{\boldsymbol{\omega}}\right)\right)\right]^T + \lambda_{\min}\left(\boldsymbol{K}_I^{\frac{1}{2}}\right)\lambda_{\min}\left((\boldsymbol{J}_{\text{tot}}^{B_{CM}})^{-1}\boldsymbol{K}_I^{\frac{1}{2}} + \boldsymbol{K}_I^{\frac{1}{2}}(\boldsymbol{J}_{\text{tot}}^{B_{CM}})^{-1}\right)}. \tag{27}$$

Therefore, the matrix $(\boldsymbol{\Xi F})_{\text{sym}}$ is negative definite if b is chosen such that $0 < b < \min(\lambda_{\max}^{\frac{1}{2}}(\boldsymbol{J}_{\text{tot}}^{B_{CM}}), \frac{\lambda_{\min}(\boldsymbol{K}_m+\boldsymbol{K}_m^T)}{2\lambda_{\max}(\boldsymbol{K}_I^{\frac{1}{2}})}, b_3)$. Let us define the generalized virtual displacement $\delta\boldsymbol{z} = [\delta\boldsymbol{\omega}_e,\, \delta\boldsymbol{y}_1]^T$, where $\delta\boldsymbol{\omega}_e$ and $\delta\boldsymbol{y}_1$ are infinitesimal displacements at fixed time. Therefore,

$$\frac{d}{dt}\left(\delta\boldsymbol{z}^T\boldsymbol{\Xi}\delta\boldsymbol{z}\right) = \delta\boldsymbol{z}^T\left((\boldsymbol{\Xi F}) + (\boldsymbol{\Xi F})^T\right)\delta\boldsymbol{z} \leq 2\lambda_{\max}((\boldsymbol{\Xi F})_{\text{sym}})\|\delta\boldsymbol{z}\|_2^2 \leq \frac{2\lambda_{\max}((\boldsymbol{\Xi F})_{\text{sym}})}{\lambda_{\max}(\boldsymbol{\Xi})}\left(\delta\boldsymbol{z}^T\boldsymbol{\Xi}\delta\boldsymbol{z}\right). \tag{28}$$

Hence, it follows from the contraction analysis that all system trajectories converge exponentially fast to a single trajectory ($\delta\boldsymbol{z} \to 0$ and $\delta\boldsymbol{\omega}_e \to 0$) at a rate of $\frac{-\lambda_{\max}((\boldsymbol{\Xi F})_{\text{sym}})}{\lambda_{\max}(\boldsymbol{\Xi})}$.[13] Moreover, in the presence of bounded time-varying resultant disturbance $\boldsymbol{d}_{\text{res},1}$ with bounded $\dot{\boldsymbol{d}}_{\text{res},1}$, we get from Lemma 4[13] that:

$$\lim_{t\to\infty}\int_0^{\boldsymbol{\omega}_e}\|\delta\boldsymbol{\omega}_e\|_2 \leq \frac{(b+1)\lambda_{\max}(\boldsymbol{\Xi})}{-\lambda_{\max}((\boldsymbol{\Xi F})_{\text{sym}})}\left(\sup_t \lambda_{\max}(\boldsymbol{K}_I^{-\frac{1}{2}})\right)\left(\sup_t\|\dot{\boldsymbol{d}}_{\text{res},1}\|_2\right). \tag{29}$$

where $\|\delta\boldsymbol{\omega}_e\|_2 \leq \|\delta\boldsymbol{z}\|_2$ and $\lambda_{\min}(\boldsymbol{\Xi}) > 1$ are used. Also, note that the disturbance term in the righthand side of (24) is $(\boldsymbol{0}; -\boldsymbol{K}_I^{-\frac{1}{2}}\dot{\boldsymbol{d}}_{\text{res},1})$. The fact that convergence of $\boldsymbol{\omega}_e \to \boldsymbol{0}$ implies convergence of the system's trajectory to the desired trajectory ($\hat{\boldsymbol{q}} \to \boldsymbol{q}_d$) is already presented in the proof of Theorem 1.

Let us now consider the case where both $\boldsymbol{K}_I$ and $\dot{\boldsymbol{K}}_I$ are uniformly positive definite diagonal matrices. The matrix $\dot{\boldsymbol{K}}_I$ can also be decomposed into $\dot{\boldsymbol{K}}_I = \dot{\boldsymbol{K}}_I^{\frac{1}{2}}\dot{\boldsymbol{K}}_I^{\frac{1}{2}}$. Let us introduce another term $\boldsymbol{y}_2$, where $\dot{\boldsymbol{y}}_2$ is defined as:

$$\dot{\boldsymbol{y}}_2 = \boldsymbol{K}_I^{\frac{1}{2}}\boldsymbol{\omega}_e - \boldsymbol{K}_I^{-\frac{1}{2}}\dot{\boldsymbol{K}}_I^{\frac{1}{2}}\boldsymbol{y}_2\,. \tag{30}$$

Once again, $\dot{\boldsymbol{\omega}}_e$ can be written in a form similar to that of Eq. (23). The matrix form of these equations is given by:

$$\begin{bmatrix}\dot{\boldsymbol{\omega}}_e\\ \dot{\boldsymbol{y}}_2\end{bmatrix} = \underbrace{\begin{bmatrix}-(\boldsymbol{J}_{\text{tot}}^{B_{CM}})^{-1}\left(\boldsymbol{K}_m - \boldsymbol{S}\left(\boldsymbol{J}_{\text{tot}}^{B_{CM}}\hat{\boldsymbol{\omega}}\right)\right) & -(\boldsymbol{J}_{\text{tot}}^{B_{CM}})^{-1}\boldsymbol{K}_I^{\frac{1}{2}}\\ \boldsymbol{K}_I^{\frac{1}{2}} & -\boldsymbol{K}_I^{-\frac{1}{2}}\dot{\boldsymbol{K}}_I^{\frac{1}{2}}\end{bmatrix}}_{\tilde{\boldsymbol{F}}}\begin{bmatrix}\boldsymbol{\omega}_e\\ \boldsymbol{y}_2\end{bmatrix} \tag{31}$$

Clearly, the symmetric part of the matrix $\boldsymbol{\Xi}\tilde{\boldsymbol{F}}$ is negative definite. Therefore,

$$\frac{d}{dt}\left(\delta\boldsymbol{z}^T\boldsymbol{\Xi}\delta\boldsymbol{z}\right) = \delta\boldsymbol{z}^T\left((\boldsymbol{\Xi}\tilde{\boldsymbol{F}}) + (\boldsymbol{\Xi}\tilde{\boldsymbol{F}})^T\right)\delta\boldsymbol{z} \leq 2\lambda_{\max}((\boldsymbol{\Xi}\tilde{\boldsymbol{F}})_{\text{sym}})\|\delta\boldsymbol{z}\|_2^2 \leq \frac{2\lambda_{\max}((\boldsymbol{\Xi}\tilde{\boldsymbol{F}})_{\text{sym}})}{\lambda_{\max}(\boldsymbol{J}_{\text{tot}}^{B_{CM}})}\left(\delta\boldsymbol{z}^T\boldsymbol{\Xi}\delta\boldsymbol{z}\right), \tag{32}$$

where $(\boldsymbol{\Xi}\tilde{\boldsymbol{F}})_{\text{sym}} = \frac{(\boldsymbol{\Xi}\tilde{\boldsymbol{F}})+(\boldsymbol{\Xi}\tilde{\boldsymbol{F}})^T}{2}$. Also, $\lambda_{\max}((\boldsymbol{\Xi}\tilde{\boldsymbol{F}})_{\text{sym}}) < 0$ and is bounded as $\lambda_{\max}((\boldsymbol{\Xi}\tilde{\boldsymbol{F}})_{\text{sym}}) \leq -\min\left(\lambda_{\min}(\boldsymbol{K}_m), \inf_t\left(\lambda_{\min}(\boldsymbol{K}_I^{-\frac{1}{2}}\dot{\boldsymbol{K}}_I^{\frac{1}{2}})\right)\right)$. Hence, it follows from the contraction analysis that all system trajectories converge exponentially fast to a single trajectory at a rate of $\frac{-\lambda_{\max}((\boldsymbol{\Xi}\tilde{\boldsymbol{F}})_{\text{sym}})}{\lambda_{\max}(\boldsymbol{J}_{\text{tot}}^{B_{CM}})}$. Moreover, in the presence of bounded $\boldsymbol{d}_{\text{res},1}$ and $\dot{\boldsymbol{d}}_{\text{res},1}$, we get from Lemma 4[13] that:

$$\lim_{t\to\infty}\int_0^{\boldsymbol{\omega}_e}\|\delta\boldsymbol{\omega}_e\|_2 \leq \frac{\lambda_{\max}(\boldsymbol{J}_{\text{tot}}^{B_{CM}})}{-\lambda_{\max}((\boldsymbol{\Xi}\tilde{\boldsymbol{F}})_{\text{sym}})}\left(\sup_t \lambda_{\max}(\boldsymbol{K}_I^{-\frac{1}{2}})\right)\left(\sup_t\|\dot{\boldsymbol{d}}_{\text{res},1}\|_2\right). \tag{33}$$

where $\|\delta\boldsymbol{\omega}_e\|_2 \leq \|\delta\boldsymbol{z}\|_2$ and $\lambda_{\min}(\boldsymbol{J}_{\text{tot}}^{B_{CM}}) > 1$ are used. Also, note that the disturbance term in the righthand side of (31) is $(\boldsymbol{0}; \boldsymbol{K}_I^{-\frac{1}{2}}\dot{\boldsymbol{d}}_{\text{res},1})$. ■

Nonlinear Adaptive Control

It is known that adaptive control can be interpreted as an intergral control scheme. Hence, the stability characteristic of an adaptive control version of the proposed Eq. (9) is similar to that of the integral control

in Section . Let the parameter $\hat{\boldsymbol{a}}$ capture the six uncertain terms in the inertia tensor $\boldsymbol{J}_{\text{tot}}^{B_{CM}}$. The resulting adaptive nonlinear tracking control law and the tuning law are given by:[14]

$$\boldsymbol{u}_c = \boldsymbol{Y}\hat{\boldsymbol{a}} - \boldsymbol{K}_r(\hat{\boldsymbol{\omega}} - \boldsymbol{\omega}_r)\,, \qquad \dot{\hat{\boldsymbol{a}}} = -\boldsymbol{\Gamma}_r \text{Proj}\left(\hat{\boldsymbol{a}}, \boldsymbol{Y}^T(\hat{\boldsymbol{\omega}} - \boldsymbol{\omega}_r)\right)\,, \tag{34}$$

where $\boldsymbol{Y}\hat{\boldsymbol{a}} = \hat{\boldsymbol{J}}_{\text{tot}}^{B_{CM}}\dot{\boldsymbol{\omega}}_r - \boldsymbol{S}\left(\hat{\boldsymbol{J}}_{\text{tot}}^{B_{CM}}\hat{\boldsymbol{\omega}}\right)\boldsymbol{\omega}_r$, $\boldsymbol{\omega}_r$ is defined in Eq. (9), and $\boldsymbol{\Gamma}_r \in \mathbb{R}^{6\times 6}$ is a positive-definite diagonal matrix. The stability result of adaptive control, unless we add a damping term to the adaptation law, is only globally asymptotic because its closed-loop system of the states $(\boldsymbol{\omega}_e, \hat{\boldsymbol{a}})^T$ yields a negative semidefinite Jacobian matrix $\left[\begin{smallmatrix} -\boldsymbol{K}_r & \boldsymbol{0} \\ \boldsymbol{0} & \boldsymbol{0} \end{smallmatrix}\right]$, similar to Eq. (24) of the integral control.

Robust Nonlinear Tracking Control Law on SO(3)

The rotation matrix ($\boldsymbol{R} \in \text{SO}(3)$) is a global and unique attitude representation. The nonlinear tracking control law Eq. (9) guarantees global exponential stability where the meaning of global convergence is valid on the domain of the particular attitude representation $\boldsymbol{q}$ (e.g., MRP, Euler angles, and quaternions) used for the control law. In this section, we present a variation of Eq. (9) that exponentially stabilizes the attitude dynamics from almost all initial conditions on SO(3), i.e., all initial conditions except those starting from a two-dimensional subset of SO(3).

It is shown in Ref. 24 that even global asymptotic convergence is not possible for any continuous feedback control law in SO(3). An almost-globally asymptotically stabilizing control law on SO(3) is discussed in Ref. 25. In this paper, we present a novel control law that guarantees exponential convergence to the desired trajectory for almost all initial conditions on SO(3). Another control law that also guarantees almost-global exponential convergence is presented in Ref. 21, but our control law and proof techniques are substantially different from the Lyapunov-based approach used in Ref. 21.

Let $\boldsymbol{R}_d(t) \in \text{SO}(3)$ denote the desired attitude trajectory, which is obtained from the desired attitude trajectory $\boldsymbol{q}_d(t)$. Let the inverse of the $\boldsymbol{S}(\cdot)$ map be the $\vee(\cdot)$ map, whose input is a skew-symmetric matrix and is defined as $\vee(\boldsymbol{S}(\boldsymbol{\omega})) = \boldsymbol{\omega}$. Let us now define the following notations:[21]

$$\boldsymbol{e}_{\hat{\boldsymbol{R}}} = \frac{1}{2\sqrt{1 + \text{tr}(\boldsymbol{R}_d^T\hat{\boldsymbol{R}})}}\left(\vee\left(\boldsymbol{R}_d^T\hat{\boldsymbol{R}} - \hat{\boldsymbol{R}}^T\boldsymbol{R}_d\right)\right)\,, \qquad \boldsymbol{e}_{\hat{\boldsymbol{\omega}}} = \hat{\boldsymbol{\omega}} - \hat{\boldsymbol{R}}^T\boldsymbol{R}_d\left(\vee\left(\boldsymbol{R}_d^T\dot{\boldsymbol{R}}_d\right)\right)\,, \tag{35}$$

where $\text{tr}(\cdot)$ is the trace of the matrix. Here $\boldsymbol{e}_{\hat{\boldsymbol{R}}}$ represents the attitude error vector between the current measured attitude $\hat{\boldsymbol{R}}$ and the desired attitude $\boldsymbol{R}_d$. For any $\boldsymbol{R}_d^T\hat{\boldsymbol{R}}$, its trace is bounded by $-1 \leq \text{tr}(\boldsymbol{R}_d^T\hat{\boldsymbol{R}}) \leq 3$. Hence $\boldsymbol{e}_{\hat{\boldsymbol{R}}}$ is not defined only on the two-dimensional subset of SO(3) where $\text{tr}(\boldsymbol{R}_d^T\hat{\boldsymbol{R}}) = -1$, i.e., $\hat{\boldsymbol{R}} = \boldsymbol{R}_d\exp(\pm\pi\boldsymbol{S}(\boldsymbol{\kappa}))$, where $\boldsymbol{\kappa} \in \mathbb{S}^2$.[21] Finally, let us define the matrix $\boldsymbol{E}(\hat{\boldsymbol{R}}, \boldsymbol{R}_d)$ as follows:[21]

$$\frac{d\boldsymbol{e}_{\hat{\boldsymbol{R}}}}{dt} = \frac{1}{2\sqrt{1 + \text{tr}(\boldsymbol{R}_d^T\hat{\boldsymbol{R}})}}\left(\text{tr}(\hat{\boldsymbol{R}}^T\boldsymbol{R}_d)\mathbf{I} - \hat{\boldsymbol{R}}^T\boldsymbol{R}_d + 2\boldsymbol{e}_{\hat{\boldsymbol{R}}}\boldsymbol{e}_{\hat{\boldsymbol{R}}}^T\right)\boldsymbol{e}_{\hat{\boldsymbol{\omega}}} = \boldsymbol{E}(\hat{\boldsymbol{R}}, \boldsymbol{R}_d)\boldsymbol{e}_{\hat{\boldsymbol{\omega}}}\,. \tag{36}$$

Theorem 3. For the given desired attitude trajectory $\boldsymbol{R}_d(t) \in \text{SO}(3)$ and positive definite matrices $\boldsymbol{K}_e \in \mathbb{R}^{3\times 3}$ and $\boldsymbol{\Lambda}_e \in \mathbb{R}^{3\times 3}$, we define the following control law:

$$\begin{aligned} \boldsymbol{u}_c &= \hat{\boldsymbol{J}}_{\text{tot}}^{B_{CM}}\dot{\boldsymbol{\omega}}_r - \boldsymbol{S}\left(\hat{\boldsymbol{J}}_{\text{tot}}^{B_{CM}}\hat{\boldsymbol{\omega}}\right)\boldsymbol{\omega}_r - \boldsymbol{K}_e(\hat{\boldsymbol{\omega}} - \boldsymbol{\omega}_r)\,, \\ \text{where} \quad \boldsymbol{\omega}_r &= \hat{\boldsymbol{R}}^T\boldsymbol{R}_d\left(\vee\left(\boldsymbol{R}_d^T\dot{\boldsymbol{R}}_d\right)\right) - \boldsymbol{\Lambda}_e\boldsymbol{E}^T(\hat{\boldsymbol{R}}, \boldsymbol{R}_d)\boldsymbol{e}_{\hat{\boldsymbol{R}}}\,. \end{aligned} \tag{37}$$

In the absence of disturbances or uncertainties, this control law guarantees exponential convergence of the system's trajectory $\boldsymbol{R}(t) \in \text{SO}(3)$ to the desired trajectory $\boldsymbol{R}_d(t)$ for almost all initial conditions, i.e., all initial conditions that are not on the two-dimensional subset of SO(3) where $\hat{\boldsymbol{R}}(0) = \boldsymbol{R}_d(0)\exp(\pm\pi\boldsymbol{S}(\boldsymbol{\kappa}))$, where $\boldsymbol{\kappa} \in \mathbb{S}^2$. Moreover, in the presence of bounded disturbances or uncertainties, this control law guarantees the system's trajectory will exponentially converge to a bounded error ball around the desired trajectory $\boldsymbol{R}_d(t)$.

Proof: The closed-loop dynamics obtained by substituting $\boldsymbol{u}_c$ from Eq. (37) into Eq. (6) is the same as Eq. (10) in the proof of Theorem 1. Hence we can directly conclude from that proof that all system trajectories of $\boldsymbol{\omega}_e$ converge exponentially fast to a single trajectory ($\boldsymbol{\omega}_e \to 0$) at a rate of $\frac{\lambda_{\min}(\boldsymbol{K}_e)}{\lambda_{\max}(\boldsymbol{J}_{\text{tot}}^{B_{CM}})}$. Moreover, in the presence of bounded resultant disturbance $\boldsymbol{d}_{\text{res},1}$, $\lim_{t\to\infty} \int_0^{\boldsymbol{\omega}_e} \|\delta \boldsymbol{y}\|_2$ is bounded by Eq. (13).

Now let us show that convergence of $\boldsymbol{\omega}_e$ implies convergence of the system's trajectory to the desired trajectory ($\boldsymbol{e}_{\hat{\boldsymbol{R}}} \to 0$). It follows from the definition of $\boldsymbol{\omega}_r$ that:

$$\boldsymbol{\omega}_e = \hat{\boldsymbol{\omega}} - \hat{\boldsymbol{R}}^T \boldsymbol{R}_d \left(\vee \left(\boldsymbol{R}_d^T \dot{\boldsymbol{R}}_d \right) \right) + \boldsymbol{\Lambda}_e \boldsymbol{E}^T \boldsymbol{e}_{\hat{\boldsymbol{R}}} = \boldsymbol{E}^{-1} \left(\dot{\boldsymbol{e}}_{\hat{\boldsymbol{R}}} + \boldsymbol{E} \boldsymbol{\Lambda}_e \boldsymbol{E}^T \boldsymbol{e}_{\hat{\boldsymbol{R}}} \right) . \tag{38}$$

In the absence of $\boldsymbol{\omega}_e$, all system trajectories of $\delta \boldsymbol{e}_{\hat{\boldsymbol{R}}}$ will converge exponentially fast to a single trajectory ($\delta \boldsymbol{e}_{\hat{\boldsymbol{R}}} \to 0$) with a rate of $\lambda_{\min}(\boldsymbol{E}\boldsymbol{\Lambda}_e\boldsymbol{E}^T)$, where $\boldsymbol{E}\boldsymbol{\Lambda}_e\boldsymbol{E}^T$ is also a positive definite matrix. In the presence of $\boldsymbol{\omega}_e$, it follows from Lemma 4[13] that:

$$\lim_{t\to\infty} \int_0^{\boldsymbol{e}_{\hat{\boldsymbol{R}}}} \|\delta \boldsymbol{e}_{\hat{\boldsymbol{R}}}\|_2 \leq \frac{\lambda_{\max}(\boldsymbol{J}_{\text{tot}}^{B_{CM}})}{\lambda_{\min}(\boldsymbol{E}\boldsymbol{\Lambda}_e\boldsymbol{E}^T)\lambda_{\min}(\boldsymbol{K}_e)\lambda_{\min}(\boldsymbol{J}_{\text{tot}}^{B_{CM}})} \left(\sup_t \sigma_{\max}(\boldsymbol{E}) \right) \left(\sup_t \|\boldsymbol{d}_{\text{res},1}\|_2 \right) . \tag{39}$$

Note that $\|\boldsymbol{e}_{\hat{\boldsymbol{R}}}\|_2 \to \infty$ if $\hat{\boldsymbol{R}} \to \boldsymbol{R}_d \exp(\pm\pi \boldsymbol{S}(\boldsymbol{\kappa}))$, where $\boldsymbol{\kappa} \in \mathbb{S}^2$. On the other hand, for any valid initial condition, $\|\boldsymbol{e}_{\hat{\boldsymbol{R}}}\|_2$ is always bounded and exponentially decreasing till it reaches the error ball. This implies that once the system starts from a valid initial condition, it can never go towards the two-dimensional subset of SO(3) due to exponential convergence. Hence we have shown, using a hierarchical closed-loop system, that the attitude error vector $\boldsymbol{e}_{\hat{\boldsymbol{R}}}$ exponentially converges to the error bound for almost all initial conditions (except those initial conditions in the two-dimensional subset of SO(3)). ■

Design of Fuel-Optimal Desired Attitude Trajectories

In this section, we design the desired (reference) attitude trajectory $\boldsymbol{q}_d(t)$ so that the asteroid and spacecraft combination stabilizes and reaches the desired attitude orientation $\boldsymbol{q}_{\text{final}}$ in a fuel-optimal fashion. We will present a reduced optimal control problem that can substantially simplify the original nonlinear optimal control problem:

$$\min_{\boldsymbol{q}_d(t),\, \boldsymbol{\omega}_d(t),\, \boldsymbol{u}_d(t)} \int_0^{t_{\text{final}}} \|\boldsymbol{u}_d(t)\|_1 dt \,, \tag{40}$$

$$\text{subject to} \quad \hat{\boldsymbol{J}}_{\text{tot}}^{B_{CM}} \dot{\boldsymbol{\omega}}_d(t) - \left(\hat{\boldsymbol{J}}_{\text{tot}}^{B_{CM}} \boldsymbol{\omega}_d(t) \right) \times \boldsymbol{\omega}_d(t) - \hat{\boldsymbol{B}} \boldsymbol{u}_d(t) = 0 \,, \tag{41}$$

$$\dot{\boldsymbol{q}}_d(t) = \boldsymbol{Z}(\boldsymbol{q}_d(t))\boldsymbol{\omega}_d(t), \qquad \boldsymbol{q}_d(0) = \boldsymbol{q}_{\text{init}} \,, \qquad \boldsymbol{q}_d(t_{\text{final}}) = \boldsymbol{q}_{\text{final}} \,, \tag{42}$$

$$\|\boldsymbol{u}_d(t)\|_\infty \leq u_{\max} \,, \qquad \|\boldsymbol{\omega}_d(t)\|_2 \leq \varepsilon_{\text{trans}} \,, \qquad \boldsymbol{\omega}_d(0) = \boldsymbol{\omega}_{\text{init}} \,, \qquad \boldsymbol{\omega}_d(t_{\text{final}}) = \boldsymbol{0} \tag{43}$$

where $\boldsymbol{\omega}_d(t)$ and $\boldsymbol{u}_d(t)$ are the fuel-optimal angular velocity and thruster input trajectories.

It is shown in Fig. 3(e) (Section) that a comparatively negligible amount of fuel is needed for orientating the system to the desired attitude after the angular velocity of the system has stabilized. In this paper, we first find only the fuel-optimal angular velocity trajectory that stabilizes the system and control the system using this desired trajectory. Once the angular velocity of the system is sufficiently close to zero, we augment this fuel-optimal angular velocity trajectory to achieve convergence to the desired attitude. The desired fuel-optimal angular velocity trajectory $\boldsymbol{\omega}_d(t)$ is obtained by solving the following reduced optimal control problem:

$$\min_{\boldsymbol{\omega}_d(t),\, \boldsymbol{u}_d(t)} \int_0^{t_{\text{final}}} \|\boldsymbol{u}_d(t)\|_1 dt \,, \qquad \text{subject to} \quad \text{Eqs. (41) and (43)} \tag{44}$$

Since the reduced optimal control problem to find $\boldsymbol{\omega}_d(t)$ in Eq. (44) has fewer constraints compared to the full optimal control problem to find both $\boldsymbol{q}_d(t)$ and $\boldsymbol{\omega}_d(t)$ in Eq. (40), it is guaranteed that the solution of

the reduced problem in Eq. (44) consumes less fuel than the full problem in Eq. (40). The desired attitude trajectory $\boldsymbol{q}_d(t)$ is then obtained using the following equations:

$$\dot{\boldsymbol{q}}_d(t) = Z(\boldsymbol{q}_d(t))\boldsymbol{\omega}_d(t)\,, \qquad \ddot{\boldsymbol{q}}_d(t) = \dot{Z}(\boldsymbol{q}_d(t))\boldsymbol{\omega}_d(t) + Z(\boldsymbol{q}_d(t))\dot{\boldsymbol{\omega}}_d(t)\,. \tag{45}$$

Note that the desired attitude trajectory $\boldsymbol{q}_d(t)$ obtained using Eq. (45) only stabilizes the angular velocity of the system. Once the angular velocity of the system is sufficiently close to zero, the desired angular velocity trajectory $\boldsymbol{\omega}_d(t)$ is augmented with a position error term so that the system's attitude converges to the desired attitude:

$$\tilde{\boldsymbol{\omega}}_d(t) = \boldsymbol{\omega}_d(t) - k_{qd} Z(\boldsymbol{q}_d(t))^{-1}(\boldsymbol{q}_d(t) - \boldsymbol{q}_{\text{final}})\,, \tag{46}$$

where $k_{qd} > 0$. The desired attitude trajectory $\boldsymbol{q}_d(t)$ is then obtained from the augmented angular velocity $\tilde{\boldsymbol{\omega}}_d(t)$ using the following equations:

$$\dot{\boldsymbol{q}}_d(t) = Z(\boldsymbol{q}_d(t))\tilde{\boldsymbol{\omega}}_d(t) = Z(\boldsymbol{q}_d(t))\boldsymbol{\omega}_d(t) - k_{qd}(\boldsymbol{q}_d(t) - \boldsymbol{q}_{\text{final}})\,, \tag{47}$$

$$\ddot{\boldsymbol{q}}_d(t) = \frac{d}{dt} Z(\boldsymbol{q}_d(t))\tilde{\boldsymbol{\omega}}_d(t) = \dot{Z}(\boldsymbol{q}_d(t))\boldsymbol{\omega}_d(t) + Z(\boldsymbol{q}_d(t))\dot{\boldsymbol{\omega}}_d(t) - k_{qd}\dot{\boldsymbol{q}}_d(t)\,. \tag{48}$$

These equations are initialized and periodically reset using the current attitude and angular velocity measurements.

Design of Desired Attitude Trajectories using Derivative plus Proportional-Derivative Control

In this section, we first state the derivative plus proportional-derivative (D+PD) control strategy, which uses derivative control followed by proportional-derivative control. We then design another desired attitude trajectory $\boldsymbol{q}_d(t)$ for the nonlinear attitude tracking control laws given in Section , based on the D+PD control strategy. As shall be seen in Section , such a desired trajectory is especially useful for minimizing the resultant disturbance torque in the presence of large modeling errors (e.g., large $\Delta \boldsymbol{J}_{\text{tot}}^{B_{CM}}$).

In the D+PD control strategy, we first use the derivative (rate damping) linear control law that guarantees global exponential stability for despinning the tumbling asteroid and spacecraft combination. It is seen that the majority of the control effort (fuel cost) is used for despinning the tumbling system. Once the angular velocity (spin rate) of the asteroid and spacecraft combination is sufficiently close to zero, the D+PD control strategy switches to a linear PD control law to stabilize the attitude of the asteroid and spacecraft combination in the desired orientation. Note that the proportional-derivative linear control law only guarantees global asymptotic stability of the system. Hence, the error in the system's trajectory may not be bounded for certain class of disturbances.[20]

Theorem 4. [15, 26, 27] (i) For the positive-definite symmetric matrix $\boldsymbol{K}_d \in \mathbb{R}^{3\times 3}$, the derivative (rate damping) control law is given by:

$$\boldsymbol{u}_c = -\boldsymbol{K}_d \hat{\boldsymbol{\omega}}\,, \tag{49}$$

In the absence of disturbances or uncertainties, this control law guarantees exponential convergence of the system's angular velocity to $\boldsymbol{0}$ rad sec^{-1}. In the presence of resultant disturbance torque, this control law guarantees the system's angular velocity trajectory will globally exponentially converge to a bounded error ball around $\boldsymbol{0}$ rad sec^{-1}.
(ii) For the positive-definite symmetric matrix $\boldsymbol{K}_d \in \mathbb{R}^{3\times 3}$ and the constant $k_p > 0$, the proportional-derivative control law is given by:

$$\boldsymbol{u}_c = -k_p \boldsymbol{\beta}_{\text{error},v} - \boldsymbol{K}_d \hat{\boldsymbol{\omega}}\,, \tag{50}$$

where the error quaternion $(\boldsymbol{\beta}_{\text{error},v}, \beta_{\text{error},4}) \in \mathbb{R}^3 \times \mathbb{R}$ represents the orientation error of $\mathcal{F}_B$ with respect to the desired target attitude $\boldsymbol{\beta}_{\text{final}}$. This control law only guarantees global asymptotic convergence of the system's trajectory to the desired trajectory $\boldsymbol{q}_d(t)$ in the absence of disturbances or uncertainties.

The global asymptotic stability of the proportional-derivative control law for the EL system (16) is also given in Refs. 14, 28. It is seen in Section that the D+PD control strategy experiences a smaller resultant disturbance torque even in the presence of large $\Delta \boldsymbol{J}_{\text{tot}}^{B_{CM}}$. Hence, we now present the design of a resultant disturbance minimizing desired attitude trajectory for the nonlinear attitude tracking control law Eq. (9).

The desired trajectory is basically broken into two phases. In the first phase, similar to the D+PD control strategy, the desired attitude trajectory is such that $\boldsymbol{\omega}_r = \mathbf{0}$ in Eq. (9) if the magnitude of the system's angular velocity is large. This ensures that the robust nonlinear tracking control law Eq. (9) effectively reduces to the linear derivative control law Eq. (49) with the same global exponential tracking stability and the resultant disturbance during this stage is as small as that of the D+PD control strategy as stated in Section .

In the second phase, once the angular velocity of the asteroid and spacecraft combination is sufficiently close to zero, we use the following desired attitude trajectory for the nonlinear tracking control law Eq. (9):

$$\boldsymbol{q}_d(t) = \boldsymbol{q}_{\text{final}}\,, \qquad \dot{\boldsymbol{q}}_d(t) = \mathbf{0}\,, \qquad \therefore \boldsymbol{\omega}_r = \boldsymbol{Z}^{-1}(\hat{\boldsymbol{q}})\boldsymbol{\Lambda}_r(\boldsymbol{q}_{\text{final}} - \hat{\boldsymbol{q}}). \tag{51}$$

Note that this ensures that the system's attitude globally exponentially converges to the desired final attitude and the system is robust to disturbances. Since the actual angular velocity of the system is small, the resultant disturbance torque is also small even in the presence of large modeling error in $\Delta\boldsymbol{J}_{\text{tot}}^{B_{CM}}$.

In this section, we presented a novel robust nonlinear tracking control law, discussed a number of extensions of this control law, and discussed two desired attitude trajectories. We study the performance of these control laws in Section . In the next section, we conduct a detailed study of the resultant disturbance torques for these control laws.

IMPACT OF FEED-FORWARD CANCELLATION ON THE RESULTANT DISTURBANCE TORQUE

In this section, we study the resultant disturbance torque for the different control laws. When a control law acts on a system with modeling errors and uncertainties, the control law can only guarantee exponential/asymptotic stability of the known part of the system. The remaining unknown terms, which the control law cannot account for, appear as a resultant disturbance torque on the system. We show in Example 1 that nonlinear control laws that use feed-forward cancellation are not suitable for this mission due to huge resultant disturbance torques. In Proposition 5, we outline a framework for minimizing the resultant disturbance torque for the robust nonlinear tracking control law Eq. (9).

The D+PD control strategy Eqs. (49,50) has $\boldsymbol{d}_{\text{res}}$ (defined in Eq. (6)) as its resultant disturbance torque. Similarly, the proposed robust nonlinear tracking laws and its extensions have $\boldsymbol{d}_{\text{res},1}$ (defined in Eq. (10)) as their resultant disturbance torque. The resultant disturbance torque for nonlinear control laws that use feed-forward cancellation is given by $\boldsymbol{d}_{\text{res},2} = \left[\boldsymbol{d}_{\text{res}} - \Delta\boldsymbol{J}_{\text{tot}}^{B_{CM}}\dot{\hat{\boldsymbol{\omega}}} - \boldsymbol{S}\left(\Delta\boldsymbol{J}_{\text{tot}}^{B_{CM}}\hat{\boldsymbol{\omega}}\right)\hat{\boldsymbol{\omega}}\right]$.

Example 1. We numerically compare the magnitude of some of the terms in the resultant disturbance torques $\boldsymbol{d}_{\text{res}}$ in Eq. (6), $\boldsymbol{d}_{\text{res},1}$ in Eq. (10), and $\boldsymbol{d}_{\text{res},2}$. Table 1 shows this comparison. The magnitude of the disturbance

Table 1. Magnitude of some of the disturbance terms in the resultant disturbance torques

Disturbance term	Magnitude (ℓ_2-norm)	Disturbance term present in		
		$\boldsymbol{d}_{\text{res}}$ in Eq. (6)	$\boldsymbol{d}_{\text{res},1}$ in Eq. (10)	$\boldsymbol{d}_{\text{res},2}$
$\Delta\boldsymbol{J}_{\text{tot}}^{B_{CM}}\dot{\hat{\boldsymbol{\omega}}} \times \hat{\boldsymbol{\omega}}$	372.8 Nm	✗	✗	✓
$\Delta\boldsymbol{J}_{\text{tot}}^{B_{CM}}\dot{\hat{\boldsymbol{\omega}}} \times \boldsymbol{\omega}_r$	depends on $\boldsymbol{\omega}_r$	✗	✓	✗
$\boldsymbol{J}_{\text{tot}}^{B_{CM}}\Delta\dot{\boldsymbol{\omega}} \times \hat{\boldsymbol{\omega}}$	7.8 Nm	✓	✓	✓
$\Delta\boldsymbol{J}_{\text{tot}}^{B_{CM}}\Delta\dot{\boldsymbol{\omega}} \times \hat{\boldsymbol{\omega}}$	6.3 Nm	✓	✓	✓
$\boldsymbol{J}_{\text{tot}}^{B_{CM}}\dot{\hat{\boldsymbol{\omega}}} \times \Delta\boldsymbol{\omega}$	10.1 Nm	✓	✓	✓
$\Delta\boldsymbol{J}_{\text{tot}}^{B_{CM}}\dot{\hat{\boldsymbol{\omega}}} \times \Delta\boldsymbol{\omega}$	7.3 Nm	✓	✓	✓

term $(\Delta\boldsymbol{J}_{\text{tot}}^{B_{CM}}\hat{\boldsymbol{\omega}} \times \hat{\boldsymbol{\omega}})$ in Table 1 is significantly larger than the magnitude of other disturbance terms. If the maximum control torque that the conceptual ARM spacecraft can generate is $\|\boldsymbol{\tau}_{\max}\|_2 = \|\boldsymbol{B}\mathbf{1}u_{\max}\|_2 \approx 10^3$ Nm, then approximately 40% of this control torque is used to just nullify this disturbance term. Hence, control laws that have the disturbance term $(\Delta\boldsymbol{J}_{\text{tot}}^{B_{CM}}\hat{\boldsymbol{\omega}} \times \hat{\boldsymbol{\omega}})$ in their resultant disturbance torque (like the feed-forward cancellation based control law) are not suitable for an ARM mission type.

Clearly, $\boldsymbol{d}_{\text{res}}$ is the smallest resultant disturbance torque because it does not contain the terms $(\Delta \boldsymbol{J}_{\text{tot}}^{B_{CM}} \hat{\boldsymbol{\omega}} \times \hat{\boldsymbol{\omega}})$ and $(\Delta \boldsymbol{J}_{\text{tot}}^{B_{CM}} \hat{\boldsymbol{\omega}} \times \boldsymbol{\omega}_r)$. Finally, the magnitude of the resultant disturbance torque $\boldsymbol{d}_{\text{res},1}$ depends on $\boldsymbol{\omega}_r$, which in turn depends on the desired attitude trajectory. □

The D+PD control strategy, which has $\boldsymbol{d}_{\text{res}}$ as its resultant disturbance torque, does not guarantee global exponential stability (in the absence of disturbances), which is a sufficient condition for satisfying the control problem statement. Hence we justified the use of the robust nonlinear tracking control law Eq. (9) for this problem statement. The following proposition provides a framework for choosing the desired attitude trajectory for this nonlinear tracking control law, such that the resultant disturbance torque $\boldsymbol{d}_{\text{res},1}$ is as small as this smallest resultant disturbance torque $\boldsymbol{d}_{\text{res}}$.

Proposition 5. Compared to $\boldsymbol{d}_{\text{res}}$, the extra terms in $\boldsymbol{d}_{\text{res},1}$ (i.e., $\Delta \boldsymbol{J}_{\text{tot}}^{B_{CM}} \dot{\boldsymbol{\omega}}_r$ and $\Delta \boldsymbol{J}_{\text{tot}}^{B_{CM}} \hat{\boldsymbol{\omega}} \times \boldsymbol{\omega}_r$) depend on $\boldsymbol{\omega}_r$, which in turn depends on the desired attitude trajectory of the robust nonlinear tracking control law Eq. (9). Based on the modeling error in the total inertia tensor of the system $\Delta \boldsymbol{J}_{\text{tot}}^{B_{CM}}$, the desired attitude trajectory is chosen as follows: (i) If the modeling error in $\Delta \boldsymbol{J}_{\text{tot}}^{B_{CM}}$ is small (i.e., $\|\Delta \boldsymbol{J}_{\text{tot}}^{B_{CM}}\|_2 \leq 10^4$ kg m^2), then select the fuel-optimal desired attitude trajectory. (ii) Otherwise, select the desired attitude trajectory obtained from the D+PD control strategy. This will ensure that $\|\boldsymbol{d}_{\text{res},1}\|_2 \approx \|\boldsymbol{d}_{\text{res}}\|_2$, consequently minimizing the resultant disturbance torque for the robust nonlinear tracking control law Eq. (9).

Proof: The worst case angular velocity of the system is bounded by 0.5 rpm ($\approx 5 \times 10^{-2}$ rad sec^{-1}) as shown in Table 2. If the fuel-optimal desired trajectory is used, then $\|\boldsymbol{\omega}_r\|_2 \approx \|\hat{\boldsymbol{\omega}}\|_2$. If the modeling error is small (i.e., $\|\Delta \boldsymbol{J}_{\text{tot}}^{B_{CM}}\|_2 \leq 10^4$ kg m^2), then $\|\Delta \boldsymbol{J}_{\text{tot}}^{B_{CM}} \hat{\boldsymbol{\omega}} \times \boldsymbol{\omega}_r\|_2 \leq 25$ Nm. Neglecting $\dot{\boldsymbol{\omega}}_r$, which is significantly smaller than $\boldsymbol{\omega}_r$ or $\hat{\boldsymbol{\omega}}$, we see that $\|\boldsymbol{d}_{\text{res},1}\|_2 \approx \|\boldsymbol{d}_{\text{res}}\|_2$.

If the D+PD control strategy based desired attitude trajectory from Section is used, then $\boldsymbol{\omega}_r = \boldsymbol{0}$ when $\hat{\boldsymbol{\omega}}$ is large, therefore $\|\Delta \boldsymbol{J}_{\text{tot}}^{B_{CM}} \hat{\boldsymbol{\omega}} \times \boldsymbol{\omega}_r\|_2 = 0$ Nm and $\|\Delta \boldsymbol{J}_{\text{tot}}^{B_{CM}} \dot{\boldsymbol{\omega}}_r\|_2 = 0$ Nm. If $\hat{\boldsymbol{\omega}}$ is sufficiently close to $\boldsymbol{0}$ (i.e., $\|\hat{\boldsymbol{\omega}}\|_2 \leq 5 \times 10^{-4}$ rad sec^{-1} as shown in Table 4 and $\|\boldsymbol{\omega}_r\|_2 \approx \|\hat{\boldsymbol{\omega}}\|_2$), and even if the modeling error is very large (i.e., $\|\Delta \boldsymbol{J}_{\text{tot}}^{B_{CM}}\|_2 \leq 10^7$ kg m^2), we still get $\|\Delta \boldsymbol{J}_{\text{tot}}^{B_{CM}} \hat{\boldsymbol{\omega}} \times \boldsymbol{\omega}_r\|_2 \leq 2.5$ Nm. Neglecting $\dot{\boldsymbol{\omega}}_r$ again, we see that $\|\boldsymbol{d}_{\text{res},1}\|_2 \approx \|\boldsymbol{d}_{\text{res}}\|_2$. ■

In the next section, the effect of these resultant disturbance torques on the performance of the control laws is shown using numerical simulations.

SIMULATION RESULTS

In this section, we numerically compare the performance of multiple attitude control laws. The best strategy for allocating thrusts to the eight RCS thrusters, from the calculated control input $\boldsymbol{u}_c$, is to solve the following optimization problem:

$$\min_{\hat{\boldsymbol{u}}} \|\hat{\boldsymbol{u}}\|_1, \quad \text{subject to} \quad \hat{\boldsymbol{B}}\hat{\boldsymbol{u}} = \boldsymbol{u}_c\,, \qquad \|\hat{\boldsymbol{u}}\|_\infty \leq u_{\max} \tag{52}$$

Since all the thrusters generate thrust independently (and there is no gimballing of thrusters), we use the ℓ_1 cost function in Eq. (52).[29] The optimal thrust allocation problem in Eq. (52) can be solved at every time instant using linear programming. Instead, in this paper, we use the Moore–Penrose pseudoinverse of $\hat{\boldsymbol{B}}$ to allocate thrusts to the eight RCS thrusters as shown below:

$$\hat{\boldsymbol{u}} = \hat{\boldsymbol{B}}^T \left(\hat{\boldsymbol{B}}\hat{\boldsymbol{B}}^T\right)^{-1} \boldsymbol{u}_c\,. \tag{53}$$

Note that we use the right-pseudoinverse since the matrix $\hat{\boldsymbol{B}}$ has full row rank and the matrix inverse $\left(\hat{\boldsymbol{B}}\hat{\boldsymbol{B}}^T\right)^{-1}$ is well defined. We do not recommend using the left-pseudoinverse since the matrix $\left(\hat{\boldsymbol{B}}^T\hat{\boldsymbol{B}}\right)$ is usually near singular and hence its inverse may not be defined. Moreover, if optimal thrust allocation problem in Eq. (52) returns an infeasible solution due to actuator saturation, then the solution from Eq. (53) is used with adequate rescaling.

The resulting control input $\boldsymbol{u}$ is then sent to the plant. The fuel consumed by the conceptual ARM spacecraft, from time t_0 to t_f, is computed using the following equation:

$$\text{Fuel consumed} = \frac{1}{I_{sp}\, g_0} \int_{t_0}^{t_f} \|\boldsymbol{u}\|_1 dt\,, \tag{54}$$

where I_{sp} is the specific impulse of the fuel in the RCS thrusters (i.e., 287 sec for the conceptual ARM spacecraft[5]) and g_0 is the nominal acceleration due to the gravity (i.e., 9.8 m sec^{-2}).

Table 2. Simulation parameters (that are same for all simulation cases)

Type of Parameter	Value
Conceptual ARM Spacecraft Parameters	$m_{\text{sc}} = 1.6 \times 10^4$ kg, $\boldsymbol{r}^{S_{CM}/S_O} = [\ 0 \quad 0 \quad 3.0\ ]$ m, $\boldsymbol{J}_{\text{sc}}^{S_{CM}} = 10^4 \times \begin{bmatrix} 5.584 & 0 & 0 \\ 0 & 5.584 & 0 \\ 0 & 0 & 1.568 \end{bmatrix}$ kg m^2,
Asteroid Parameters	$m_{\text{ast}} = 1.2 \times 10^6$ kg, $\rho_{\text{ast}} = 1.9$ g cm^{-3}, Shape model: Eros, $\boldsymbol{J}_{\text{ast}}^{B_{CM}} = 10^7 \times \begin{bmatrix} 0.8658 & 0.4432 & -0.0005 \\ 0.4432 & 3.4900 & 0.0002 \\ -0.0005 & 0.0002 & 3.5579 \end{bmatrix}$ kg m^2, $\boldsymbol{r}^{S_O/B_{CM}} = [\ -0.0495 \quad -0.0004 \quad 3.5456\ ]$ m,
External Disturbance Actuator Error	$\|\boldsymbol{d}_{\text{ext}}\|_2 \approx 1$ Nm, $\Delta\boldsymbol{u} = 0$ N,
Initial Conditions	$\boldsymbol{q}_{\text{initial}} = [\ 0.05 \quad 0.04 \quad 0.03\ ]$, $\boldsymbol{\omega}_{\text{initial}} = [\ 0.01 \quad 0.02 \quad 0.03\ ]$ rad sec^{-1},
Desired Final Conditions Eqs. (7,8)	$\|\boldsymbol{\omega}(t)\|_2 \leq 0.5$ rpm, $\forall t \in \mathbb{R}$, $\boldsymbol{q}_{\text{final}} = [\ 0 \quad 0 \quad 0\ ]$, $\|\boldsymbol{q}(t) - \boldsymbol{q}_{\text{final}}\|_2 \leq 10^{-2}$, $\forall t > 10^5$ sec, $\|\boldsymbol{\omega}(t)\|_2 \leq 10^{-4}$ rad sec^{-1}, $\forall t > 10^5$ sec,

We assume that the ARM spacecraft captures the 1.2×10^6 kg asteroid and stabilizes the rigid asteroid and spacecraft combination from the given initial conditions to the desired final conditions. The simulation parameters, which are the same for all simulation cases, like the inertia tensors of the asteroid and spacecraft, initial and final conditions, etc. are given in Table 2. We assume that the actuators of the ARM spacecraft are precisely calibrated, hence there is no actuator error. In Table 3, we state the seven simulation cases considered in this study. These simulation cases are based on varying levels of: (i) modeling uncertainties in the estimated inertia tensor of the asteroid ($\Delta\boldsymbol{J}_{\text{ast}}^{B_{CM}}$), (ii) modeling uncertainties in the vector from the base of the ARM-spacecraft's body to the center of mass of the system ($\Delta\boldsymbol{r}^{S_O/B_{CM}}$), (iii) measurement errors in the system's angular velocity ($\Delta\boldsymbol{\omega}$), (iv) measurement errors in the system's attitude represented using MRP ($\Delta\boldsymbol{q}$), and (v) actuator saturations ($u_{\max}$). Each simulation is executed for 10^5 sec (≈ 28 hours). In Table 3, the additive measurement errors ($\Delta\boldsymbol{\omega}$, $\Delta\boldsymbol{q}$) are simulated using band-limited white noise where $\mathcal{P}(\cdot)$ specifies the height of the power spectral density of the white noise, which is the same for each axis. Note that in Case 4, the maximum thrust magnitude of each thruster ($u_{\max}$) is increased to 1000 N to avoid actuator saturation.

We compare the performance of the following attitude control laws: (i) Robust nonlinear tracking control law (Robust NTCL) Eq. (9), (ii) Adaptive version of the robust nonlinear tracking control law (Adaptive RNTCL) Eq. (34), (iii) Robust nonlinear tracking control law for Euler-Lagrangian systems (Robust NTCL for EL) Eq. (18), and (iv) Derivative plus proportional-derivative (D+PD) control strategy Eqs. 49,50). For the tracking control laws, both the fuel-optimal desired attitude trajectory (Section) and D+PD control strategy based desired attitude trajectory (Section) are considered. The control law parameters and the parameters for these two desired attitude trajectories are given in Table 4.

The performance of these control laws for the seven simulation are shown in Table 5, where the following terms are used: (a) The angular velocity convergence time $t_{\omega,\text{conv}}$ denotes the least time instant after which the system's angular velocity $\boldsymbol{\omega}(t)$ is always below the given threshold of 10^{-4} rad sec^{-1}, i.e., $\|\boldsymbol{\omega}(t)\|_2 \leq 10^{-4}$ rad sec^{-1}, $\forall t > t_{\omega,\text{conv}}$. (b) The attitude convergence time $t_{q,\text{conv}}$ denotes the least time instant after which the error in the EL system's attitude $\|\boldsymbol{q}(t) - \boldsymbol{q}_{\text{final}}\|_2$ is always below the given threshold of 10^{-2}, i.e., $\|\boldsymbol{q}(t) - \boldsymbol{q}_{\text{final}}\|_2 \leq 10^{-2}$, $\forall t > t_{q,\text{conv}}$. Note that after time $t_{q,\text{conv}}$, the attitude control law can be switched off because the asteroid and spacecraft combination has been three-axis stabilized in the final desired orientation. The fuel consumed up to time $t_{\omega,\text{conv}}$ and $t_{q,\text{conv}}$ are also shown. (c) The symbol $\mathcal{NC}$ or "Not Converged"

Table 3. Time-varying simulation parameters for the simulation cases

Case	Modeling Uncertainties		Measurement Errors		Actuator Sat.
	$\|\Delta \boldsymbol{J}_{\text{ast}}^{B_{CM}}\|_2$ (kg m^2)	$\|\Delta \boldsymbol{r}^{S_O/B_{CM}}\|_2$ (m)	$\mathcal{P}(\Delta\boldsymbol{\omega})$ (rad^2 sec^{-2})	$\mathcal{P}(\Delta \boldsymbol{q})$	$u_{\max}$ (N)
1.	0	0	0	0	200
2.	10^5	10^{-2}	0	0	200
3.	10^6	10^{-1}	0	0	200
4.	10^7	1	0	0	1000
5.	0	0	10^{-12}	10^{-8}	200
6.	0	0	10^{-10}	10^{-6}	200
7.	10^7	1	10^{-10}	10^{-6}	200

Table 4. Control law parameters and desired attitude trajectory parameters

Type of Parameter	Value
Robust NTCL Eq. (9)	$\boldsymbol{K}_r = 10^4 \times \mathbf{I}, \boldsymbol{\Lambda}_r = 10^{-3} \times \mathbf{I},$
Adaptive RNTCL Eq. (34)	$\boldsymbol{K}_r = 10^4 \times \mathbf{I}, \boldsymbol{\Lambda}_r = 10^{-3} \times \mathbf{I}, \boldsymbol{\Gamma}_r = 10^{12} \times \mathbf{I}$
Robust NTCL for EL Eq. (18)	$\boldsymbol{K}_\ell = 10^4 \times \mathbf{I}, \boldsymbol{\Lambda}_\ell = 10^{-3} \times \mathbf{I},$
D+PD Control Strategy Eqs. (49,50)	$\boldsymbol{K}_d = 10^4 \times \mathbf{I}, k_p = 10,$ Switch from derivative to proportional-derivative when $\|\dot{\tilde{\boldsymbol{\omega}}}(t)\|_2 \leq 5 \times 10^{-4}$ rad sec^{-1}.
Fuel-optimal desired attitude trajectory	Desired angular velocity $\boldsymbol{\omega}_d(t)$ is obtained by solving Eq. (44) using the GPOPS-II numerical solver[30] Desired trajectory $\boldsymbol{q}_d(t)$ obtained using Eqs. (45). When $\|\dot{\tilde{\boldsymbol{\omega}}}(t)\|_2 \leq 5 \times 10^{-4}$ rad sec^{-1}, switch to angular velocity $\tilde{\boldsymbol{\omega}}_d(t)$ in Eq. (46) with $k_{qd} = 10^{-4}$, desired trajectory $\boldsymbol{q}_d(t)$ obtained using Eqs. (47,48).
D+PD control strategy based desired attitude trajectory	Start with $\boldsymbol{\omega}_r = \mathbf{0}$. When $\|\dot{\tilde{\boldsymbol{\omega}}}(t)\|_2 \leq 5 \times 10^{-4}$ rad sec^{-1}, switch to desired trajectory $\boldsymbol{q}_d(t) = \boldsymbol{q}_{\text{final}}$ in Eq. (51), therefore $\boldsymbol{\omega}_r = \boldsymbol{Z}^{-1}(\hat{\boldsymbol{q}})\boldsymbol{\Lambda}_r(\boldsymbol{q}_{\text{final}} - \hat{\boldsymbol{q}})$.

refers to the case when the control law is not able to stabilize the system, which is usually due to actuator saturation.

In the absence of measurement errors and modeling uncertainties (see Case 1), the robust nonlinear tracking control law for EL systems Eq. (18) tracks the fuel-optimum reference trajectory and consumes the least amount of fuel among all the control laws. The robust nonlinear tracking control law Eq. (9) also consumes less fuel, and the simulation results for this case are shown in Fig. 3(a,c,e). Fig. 3(e) also shows the fuel consumption for the case where the fuel-optimal $\boldsymbol{\omega}_d(t)$ trajectory is not augmented (i.e., $k_{qd} = 0$) and consequently only the angular velocity of the system converges. We can infer from this plot that a comparatively negligible amount of fuel ($\approx$ 1 kg) is used for stabilizing the attitude of the asteroid and spacecraft combination using the augmented angular velocity $\tilde{\boldsymbol{\omega}}_d(t)$ in Eq. (46).

We conclude from Cases 2 and 3 that in the absence of measurement errors and under minor modeling uncertainties, which can be achieved using online system identification techniques, the robust nonlinear tracking control law is the best strategy because it guarantees exponential convergence to the fuel-optimal reference trajectory and consumes the least fuel. One caveat of using this control law is that the nonlinear optimal control problem in Eq. (44) should be solved in real time for the given initial angular velocity $\boldsymbol{\omega}_{\text{initial}}$ and the estimated inertia tensor of the asteroid and spacecraft combination $\hat{\boldsymbol{J}}_{\text{tot}}^{B_{CM}}$. Case 4 shows that the nonlinear control laws, which track the fuel-optimal desired attitude trajectory, consume significantly more fuel than the control laws that track the D+PD control strategy based desired attitude trajectory, due to the large resultant disturbance torque. Note that the angular velocity convergence times ($t_{\omega,\text{conv}}$) of the nonlinear control laws for Cases 1–4 are different because different values of $\hat{\boldsymbol{J}}_{\text{tot}}^{B_{CM}}$ are used in the nonlinear optimal control problem (44) to obtain the fuel-optimal desired attitude trajectories ($\boldsymbol{\omega}_d(t)$, $\boldsymbol{q}_d(t)$).

In Cases 5–7, a simple filtering algorithm is used to remove the additive noise from the measured states. In this filtering algorithm, the states ($\boldsymbol{\omega}$, $\boldsymbol{q}$) are first predicted using the nonlinear dynamics and kinematics

Table 5. Performance of control laws for the simulation cases, where the fuel-optimal and D+PD based desired attitude trajectories are used

		Fuel-optimal trajectory			D+PD based trajectory		
Case	**Convergence Time and Fuel Consumed**	**Robust NTCL Eq. (9)**	**Adaptive RNTCL Eq. (34)**	**Robust NTCL for EL Eq. (18)**	**Robust NTCL Eq. (9)**	**Adaptive RNTCL Eq. (34)**	**D+PD Control Strategy Eqs. (49,50)**
1.	$t_{\omega,\text{conv}}$ (sec)	4.44×10^4	4.53×10^4	4.44×10^4	2.34×10^4	2.34×10^4	3.08×10^4
	Fuel at $t_{\omega,\text{conv}}$ (kg)	96.2	121.7	78.7	135.2	135.1	120.2
	$t_{q,\text{conv}}$(sec)	8.08×10^4	8.06×10^4	8.65×10^4	3.01×10^4	2.93×10^4	4.31×10^4
	Fuel at $t_{q,\text{conv}}$ (kg)	96.6	122.1	79.1	135.5	135.3	121.4
2.	$t_{\omega,\text{conv}}$ (sec)	5.23×10^4	5.32×10^4	5.21×10^4	2.35×10^4	2.35×10^4	3.16×10^4
	Fuel at $t_{\omega,\text{conv}}$ (kg)	82.7	113.0	78.3	134.3	134.1	120.6
	$t_{q,\text{conv}}$(sec)	8.57×10^4	8.57×10^4	8.70×10^4	3.03×10^4	2.95×10^4	4.31×10^4
	Fuel at $t_{q,\text{conv}}$ (kg)	83.1	113.4	78.7	134.5	134.3	121.7
3.	$t_{\omega,\text{conv}}$ (sec)	2.30×10^4	2.37×10^4	2.30×10^4	2.38×10^4	2.38×10^4	3.41×10^4
	Fuel at $t_{\omega,\text{conv}}$ (kg)	138.9	130.2	116.8	127.9	127.8	121.0
	$t_{q,\text{conv}}$(sec)	5.56×10^4	5.59×10^4	5.80×10^4	3.07×10^4	2.97×10^4	4.84×10^4
	Fuel at $t_{q,\text{conv}}$ (kg)	139.4	130.8	117.3	128.2	128.1	121.6
4.	$t_{\omega,\text{conv}}$ (sec)	2.86×10^4	3.06×10^4	2.71×10^4	2.07×10^4	2.07×10^4	2.80×10^4
	Fuel at $t_{\omega,\text{conv}}$ (kg)	1220.1	814.7	753.4	115.1	115.2	116.1
	$t_{q,\text{conv}}$(sec)	6.04×10^4	6.14×10^4	7.24×10^4	2.61×10^4	2.52×10^4	4.16×10^4
	Fuel at $t_{q,\text{conv}}$ (kg)	1220.3	814.9	753.7	115.6	115.6	117.5
5.	$t_{\omega,\text{conv}}$ (sec)	4.53×10^4	4.53×10^4	4.53×10^4	2.34×10^4	2.34×10^4	3.08×10^4
	Fuel at $t_{\omega,\text{conv}}$ (kg)	96.2	122.0	78.8	135.3	135.1	120.2
	$t_{q,\text{conv}}$(sec)	8.06×10^4	8.06×10^4	8.63×10^4	3.01×10^4	2.93×10^4	4.31×10^4
	Fuel at $t_{q,\text{conv}}$ (kg)	96.5	122.3	79.2	135.5	135.3	121.5
6.	$t_{\omega,\text{conv}}$ (sec)	4.53×10^4	4.53×10^4	4.52×10^4	2.34×10^4	2.34×10^4	3.08×10^4
	Fuel at $t_{\omega,\text{conv}}$ (kg)	94.6	124.4	80.0	135.2	135.0	120.2
	$t_{q,\text{conv}}$(sec)	8.00×10^4	8.02×10^4	8.55×10^4	3.01×10^4	2.93×10^4	4.32×10^4
	Fuel at $t_{q,\text{conv}}$ (kg)	95.3	125.1	80.7	135.5	135.3	121.5
7.	$t_{\omega,\text{conv}}$ (sec)	$\mathcal{NC}^{\ddagger\ddagger}$	$\mathcal{NC}^{\ddagger\ddagger}$	$\mathcal{NC}^{\ddagger\ddagger}$	2.05×10^4	2.05×10^4	2.76×10^4
	Fuel at $t_{\omega,\text{conv}}$ (kg)				114.6	114.6	115.9
	$t_{q,\text{conv}}$(sec)	$\mathcal{NC}^{\ddagger\ddagger}$	$\mathcal{NC}^{\ddagger\ddagger}$	$\mathcal{NC}^{\ddagger\ddagger}$	2.59×10^4	2.52×10^4	4.11×10^4
	Fuel at $t_{q,\text{conv}}$ (kg)				115.1	115.1	117.3

equations and state values from the previous time instant. Then the errors between the measured states and the predicted states are filtered using a low-pass filter (first order filter with transfer function $\frac{\omega_{\text{cutoff}}}{s+\omega_{\text{cutoff}}}$, where $\omega_{\text{cutoff}} = 0.02\pi$ rad sec^{-1}) to remove the high frequency components arising from the noise. Finally the filtered errors are added to the predicted states to retrieve the estimated states ($\hat{\boldsymbol{\omega}}$, $\hat{\boldsymbol{q}}$).

Cases 5 and 6 show that the robust nonlinear control law Eq. (9), tracking the fuel-optimal trajectory, consumes less fuel than the D+PD control strategy based control laws in the presence of small measurement errors. But Case 7 shows that this robust nonlinear control law Eq. (9) cannot stabilize the system in the presence of both large measurement errors and large modeling errors, due to the large resultant disturbance torque.

If we use the resultant disturbance torque minimizing, D+PD control strategy based desired attitude tra-

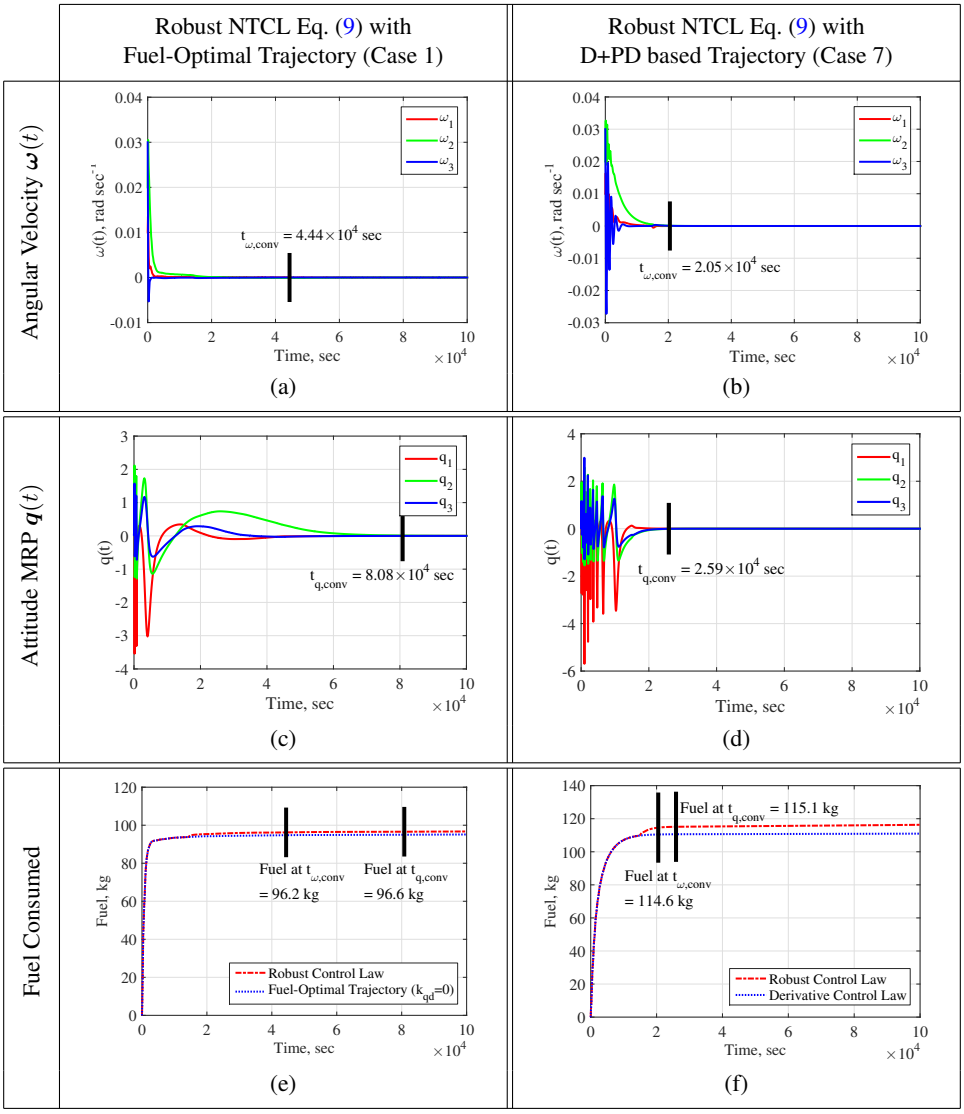

Figure 3. Simulation results of the robust nonlinear tracking control law Eq. (9) for Cases 1 and 7 are shown. The plots show the trajectories of the angular velocity $\boldsymbol{\omega}(t)$, the attitude represented using MRP $\boldsymbol{q}(t)$, and the fuel consumed with respect to time. The angular velocity convergence time $t_{\omega,\mathbf{conv}}$, the attitude convergence time $t_{q,\mathbf{conv}}$, and the corresponding fuel consumption are also shown.

jectory, then the robust nonlinear control law Eq. (9) can stabilize the system in the presence of both large measurement errors and large modeling errors, as shown in Case 7. Moreover, the fuel consumed and the time of convergence do not change much with uncertainties and errors, as seen in Cases 1–7. Moreover, Case 7 in Table 3 shows the worst case measurement errors for the desired convergence bounds because if the measurement errors (noise levels) increase above the values, then the instantaneous magnitude of the measurement errors become comparable to the desired convergence bounds in Table 2 and the ARM spacecraft expends fuel continuously to counter these errors. Therefore these uncertainty and error limits place requirements on the technical capabilities of the sensors and actuators on board the actual ARM spacecraft.

The simulation results (trajectories) of the robust nonlinear tracking control law Eq. (9) for Case 7 are shown in Fig. 3(b,d,f). Note that the net fuel consumed ($\approx$ 120 kg) after 10^5 sec is comfortably within the fuel

capacity of the conceptual ARM spacecraft (i.e., 900 kg[5]). Figure 3(f) also shows the fuel consumption for the case where only the derivative (rate damping) control law Eq. (49) is used for the entire time and consequently only the angular velocity of the system converges. We can infer from this plot that a comparatively negligible amount of fuel (≈ 5 kg) is used by the proportional term in Eq. (51) for stabilizing the attitude of the asteroid and spacecraft combination.

CONCLUSIONS

We presented a new robust nonlinear tracking control law that guarantees global exponential convergence to the desired attitude trajectory and guarantees bounded tracking errors (such as finite-gain $\mathcal{L}_p$ stability and input-to-state stability) in the presence of disturbances. The development of such a nonlinear control law was motivated by the challenge of despinning stabilization and three-axis attitude control of a tumbling asteroid and spacecraft combination that possesses large modelling uncertainty. The benefits of this new control law include superior robustness due to no feed-forward cancellation and straightforward extensions to integral control and various attitude representations such as SO(3). We then presented a detailed study of the resultant disturbance torques obtained by various attitude control law types and concluded that the control laws that use no feed-forward cancellation produce a smaller disturbance torque in the closed-loop system.

We also discussed techniques for obtaining fuel-optimal or resultant disturbance torque minimizing desired attitude trajectories for these tracking control laws. We then numerically compared the performance of multiple control laws, such as the proposed robust nonlinear tracking control law, adaptive control, the robust tracking control law for EL systems, and the D+PD linear control strategy. We illustrated that in the presence of small measurement errors and under small modeling uncertainties, which can be achieved using online system identification, the robust nonlinear tracking control law is the best strategy because it tracks the fuel-optimal reference trajectory and consumes the least amount of fuel. We also showed that a comparatively negligible amount of fuel (≈ 1 kg) is needed for orientating the system to the desired attitude after the angular velocity of the system is stabilized. One caveat of using nonlinear control tracking an optimal attitude trajectory is that the spacecraft should have sufficient computational power for online system identification and real time fuel-optimal trajectory generation.

On the other hand, in the presence of large modeling uncertainties, measurement errors, and actuator saturations, or in the absence of sufficient computational power onboard the ARM spacecraft, the simple linear D+PD control strategy resulted in good performance. This performance was further enhanced with properties of superior robustness and convergence if the robust nonlinear tracking control law was used to globally exponentially track a desired attitude trajectory generated from D+PD control. We envisage that these guidelines can be used for improving the design of the ARM spacecraft.

ACKNOWLEDGMENTS

We would like to thank A. Miguel San Martin and Gurkipal Singh for their valuable inputs. This research was supported by the Jet Propulsion Laboratory, California Institute of Technology, under a contract with the National Aeronautics and Space Administration. © 2015 California Institute of Technology.

REFERENCES

[1] Brophy, J. R. and Friedman, L., "Returning an Entire Near-Earth Asteroid in Support of Human Exploration Beyond Low-Earth Orbit," *IAF Global Exploration Conference*, Washington, D. C., May 2012.

[2] Tsuda, Y., Yoshikawa, M., Abe, M., Minamino, H., and Nakazawa, S., "System Design of the Hayabusa–2 Asteroid Sample Return Mission to 1999JU3," *Acta Astronautica*, Vol. 91, 2013, pp. 356–362.

[3] Harris, A., Barucci, M., Cano, J., Fitzsimmons, A., Fulchignoni, M., Green, S., Hestroffer, D., Lappas, V., Lork, W., Michel, P., Morrison, D., Payson, D., and Schaeffer, F., "The European Union Funded NEOSHIELD Project: A Global Approach to Near-Earth Object Impact Threat Mitigation," *Acta Astronautica*, Vol. 90, No. 1, 2013, pp. 80–84.

[4] Glassmeier, K.-H., Boehnhardt, H., Koschny, D., Kührt, E., and Richter, I., "The Rosetta Mission: Flying Towards the Origin of the Solar System," *Space Science Reviews*, Vol. 128, No. 1-4, 2007, pp. 1–21.

[5] Brophy, J., Culick, F., and Friedman, L., "Asteroid Retrieval Feasibility Study," Tech. rep., Keck Institute for Space Studies, California Institute of Technology, Pasadena, CA, April 2012.

[6] Mazanek, D. D., Brophy, J. R., and Merrill, R. G., "Asteroid Retrieval Mission Concept – Trailblazing Our Future in Space and Helping to Protect Us from Earth Impactors," *3rd IAA Planetary Defense Conf.*, Flagstaff, AZ, Apr. 2013.

[7] Merrill, R. G., Qu, M., Vavrina, M. A., Jones, C. A., and Englander, J., "Interplanetary Trajectory Design for the Asteroid Robotic Redirect Mission Alternate Approach Trade Study," *AIAA/AAS Astrodynamics Specialist Conf.*, San Diego, CA, Aug. 2014.

[8] Roithmayr, C. M., Shen, H., Jesick, M. C., and Cornelius, D. M., "Catching a Rolling Stone: Dynamics and Control of a Spacecraft and an Asteroid," *Proc. 3rd IAA Planetary Defense Conference*, Flagstaff, AZ, April 2013.

[9] Shen, H. and Roithmayr, C., "Co-Spin with Symmetry Axis Stabilization, and De-Spin for Asteroid Capture," *Amer. Control Conf.*, Portland, OR, June 2014, pp. 1599–1604.

[10] Luo, W., Chu, Y.-C., and Ling, K.-V., "Inverse Optimal Adaptive Control for Attitude Tracking of Spacecraft," *IEEE Trans. Autom. Control*, Vol. 50, No. 11, 2005, pp. 1639–1654.

[11] Junkins, J. L., Akella, M. R., and Robinett, R. D., "Nonlinear Adaptive Control of Spacecraft Maneuvers," *J. Guid. Control Dyn.*, Vol. 20, No. 6, 1997, pp. 1104–1110.

[12] Markley, F. L. and Crassidis, J. L., *Fundamentals of Spacecraft Attitude Determination and Control*, Springer, 2014.

[13] Chung, S.-J., Bandyopadhyay, S., Chang, I., and Hadaegh, F. Y., "Phase Synchronization Control of Complex Networks of Lagrangian Systems on Adaptive Digraphs," *Automatica*, Vol. 49, No. 5, May 2013, pp. 1148–1161.

[14] Slotine, J.-J. E. and Li, W., *Applied Nonlinear Control*, Vol. 199, Prentice-Hall Englewood Cliffs, NJ, 1991.

[15] Tsiotras, P., "Stabilization and Optimality Results for the Attitude Control Problem," *J. Guid. Control Dyn.*, Vol. 19, No. 4, 1996, pp. 772–779.

[16] Chung, S.-J., Ahsun, U., and Slotine, J.-J. E., "Application of Synchronization to Formation Flying Spacecraft: Lagrangian Approach," *J. Guid. Control Dyn.*, Vol. 32, No. 2, Mar.-Apr. 2009, pp. 512–526.

[17] Sidi, M. J., *Spacecraft Dynamics and Control*, Cambridge Univ. Press, Cambridge, U.K., 1997.

[18] Wie, B., *Space Vehicle Dynamics and Control*, AIAA, Reston, VA, US, 1998.

[19] Shuster, M. D., "A Survey of Attitude Representations," *Navigation*, Vol. 8, No. 9, 1993.

[20] Khalil, H. K., *Nonlinear Systems*, Macmillan Pub. Co., New York, 1992.

[21] Lee, T., "Exponential Stability of an Attitude Tracking Control System on SO(3) for Large-Angle Rotational Maneuvers," *Syst. Control Lett.*, Vol. 61, No. 1, 2012, pp. 231–237.

[22] Lohmiller, W. and Slotine, J. E., "On Contraction Analysis for Nonlinear Systems," *Automatica*, Vol. 34, No. 6, 1998, pp. 683 – 696.

[23] Wang, W. and Slotine, J.-J. E., "On Partial Contraction Analysis for Coupled Nonlinear Oscillators," *Biological cybernetics*, Vol. 92, No. 1, 2005, pp. 38–53.

[24] Bhat, S. P. and Bernstein, D. S., "A Topological Obstruction to Continuous Global Stabilization of Rotational Motion and the Unwinding Phenomenon," *Systems & Control Letters*, Vol. 39, No. 1, 2000, pp. 63–70.

[25] Chaturvedi, N. A., Sanyal, A. K., and McClamroch, N. H., "Rigid–Body Attitude Control," *IEEE Control Syst. Mag.*, Vol. 31, No. 3, 2011, pp. 30–51.

[26] Schaub, H. and Junkins, J. L., "Stereographic Orientation Parameters for Attitude Dynamics: A Generalization of the Rodrigues Parameters," *Journal of the Astronautical Sciences*, Vol. 44, No. 1, Jan.–Mar. 1996, pp. 1–19.

[27] Wie, B. and Barba, P. M., "Quaternion Feedback for Spacecraft Large Angle Maneuvers," *J. Guid. Control Dyn.*, Vol. 8, No. 3, 1985, pp. 360–365.

[28] Chung, S.-J. and Slotine, J. J. E., "Cooperative Robot Control and Concurrent Synchronization of Lagrangian Systems," *IEEE Trans. Robotics*, Vol. 25, No. 3, 2009, pp. 686–700.

[29] Ross, I. M., "Space Trajectory Optimization and L1-Optimal Control Problems," *Elsevier Astrodynamics Ser.*, Vol. 1, 2007, pp. 155–158.

[30] Patterson, M. A. and Rao, A. V., "GPOPS-II: A MATLAB Software for Solving Multiple-Phase Optimal Control Problems Using hp-Adaptive Gaussian Quadrature Collocation Methods and Sparse Nonlinear Programming," *ACM Transactions on Mathematical Software*, Dec. 2013.